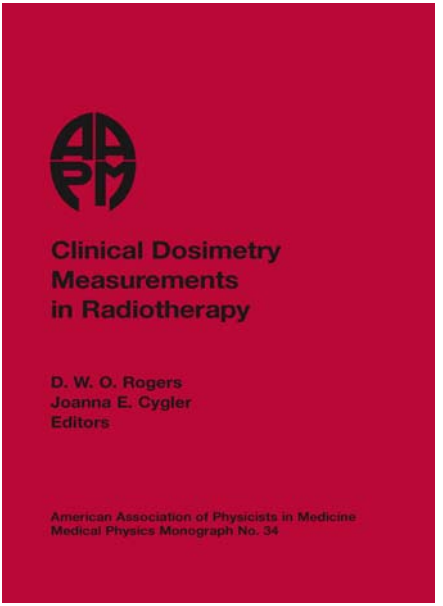

Here is a sample chapter from this book.

Chapter 9

The Physics of the AAPM's TG-51 Protocol

D. W. O. Rogers, Ph.D.
Carleton Laboratory for Radiotherapy Physics
Carleton University, Ottawa, Ontario, Canada

1. Introduction

In 1998, the AAPM approved the TG-51 protocol for reference dosimetry of high-energy photon and electron radiotherapy beams. The protocol, herein referred to simply as TG51, was published in September 1999 (Almond et al. 1999) and replaced the previous TG-21 protocol published in 1983 (AAPM TG-21) and

herein referred to simply as TG-21. The TG-51 protocol document contains a minimum of background material and is meant to explain how to do reference dosimetry accurately. Little justification is given in TG-51 for many of the steps involved in using the protocol since this would have made the document more complex. While all of the data used in the protocol come from published papers, and there have been two publications which describe most of the details of the calculations used in TG-51 (Rogers 1996, 1998), this chapter is a long-overdue effort to document and explain, in a single place, as much of the physics and computational details behind TG-51 as reasonable.

The chapter starts with an introduction to the protocol formalism and a derivation of the equations used in the formalism. This is followed by a discussion of the physical data sets used in TG-51 and the details of the calculations of the various factors used in the equations. The discussion of each correction factor includes a discussion of the current state-of-the-art for that particular factor and these sections can be skipped without loss of detail about TG-51. After this is a discussion of the equations used for ion recombination corrections. The final section presents a summary of experimental work to measure k_Q values, which can be summarized by saying that the photon beam data measured in many different primary standards laboratories agrees with the TG-51 calculated values within experimental uncertainties.

The notation used in this chapter is the same as that used in TG-51, extended where necessary by the notation used in two previous summer school presentations (Rogers 1996,1992c). Since TG-51 was published, there has been an international consensus to use the term "calibration coefficient" rather than "calibration factor" since a change of units is implied with $N_{D,w}$. This terminology is used here but there is no change in meaning from the term "calibration factor" as used in TG-51.

About 3 years after the AAPM approved the TG-51 protocol, the International Atomic Energy Agency (IAEA) published a Code of Practice which is based on very similar physics (with a few minor exceptions that will be discussed below) but a somewhat different notation (IAEA 2000). This will be referred to simply as TRS-398 (for Technical Report Series). Similarly the IAEA's 1987 Code of Practice (IAEA 1987) will be referred to as TRS-277.

2. The TG-51 Formalism

2.1 Review of the Formalism

The major new feature of TG-51 compared to the previous TG-21 protocol is that it starts from an absorbed-dose calibration coefficient rather than an exposure or air-kerma calibration coefficient. Thus TG-51 starts with $N_{D,w}^{Q}$ (in Gy/C or Gy/rdg), the absorbed-dose to water calibration coefficient for an ion chamber located in a beam of quality Q. Under reference conditions the dose is given by:

$$D_w^Q = MN_{D,w}^Q \qquad \left[\mathrm{Gy}\right], \tag{9.1}$$

where D_w^Q is the absorbed dose to water (in Gy) at the point of measurement of the ion chamber when it is absent (i.e., at the reference depth); M is the fully corrected electrometer reading in coulombs (C) or meter units (rdg) which has been corrected for ion recombination, polarity, and electrometer calibration effects and corrected to standard environmental conditions of temperature and pressure (see section 2.4.3); and the same or equivalent waterproofing sleeve is used as used during the calibration (if needed). For photon beams the beam quality, Q, is specified by $\%\mathrm{dd}(10)_x$, which is defined below. TG-51 presumes that absorbed-dose calibration coefficients will usually be obtained for reference conditions in a ^{60}Co beam, *viz.,* $N_{D,w}^{^{60}Co}$. The quality conversion factor, k_Q, is defined such that:

$$N_{D,w}^{Q} = k_Q N_{D,w}^{^{60}Co} \qquad \left[\text{Gy/C or Gy/rdg}\right], \tag{9.2}$$

i.e., k_Q converts the absorbed-dose to water calibration coefficient for a ^{60}Co beam into the calibration coefficient for an arbitrary photon or electron beam of quality Q. The quality conversion factor k_Q is chamber specific. Using k_Q, gives (Hohlfeld 1988; Rogers 1992b; Andreo 1992):

$$D_w^Q = M k_Q N_{D,w}^{^{60}Co} \qquad \left[\text{Gy}\right]. \tag{9.3}$$

For photon beams, TG-51 provides values of k_Q as a function of Q for most chambers used for reference dosimetry.

For electron beams, the beam quality, Q, is specified by R_{50}, the depth in centimeters in water at which the dose drops to 50% of its maximum. In electron beams the quality conversion factor k_Q contains two components, i.e.:

$$k_Q = P_{gr}^Q k_{R_{50}}, \tag{9.4}$$

where $k_{R_{50}}$, is a chamber-specific factor that depends on the quality for which the absorbed-dose calibration coefficient was obtained and P_{gr}^Q, the gradient correction factor (necessary only for cylindrical chambers) corrects for gradient effects at the reference depth. The P_{gr}^Q factor is necessitated by the fact that absorbed-dose calibration coefficients are defined with the chamber's point of measurement at the reference depth and by the fact that the value of P_{gr}^Q depends on the radius of the chamber cavity and the ionization gradient at the point of measurement in the user's beam. Since P_{gr}^Q can vary considerably in different clinical beams with the same R_{50}, the user must measure P_{gr}^Q in their own beam using simple methods described in TG-51. In contrast, the gradient effect in a photon beam of a given quality (i.e., a given value of $\%\mathrm{dd}(10)_x$) is always the same (and can be calculated, see section 5.5) and thus can be included in the k_Q value.

TG-51 writes $k_{R_{50}}$ as the product of two factors, *viz.*:

$$k_{R_{50}} = k'_{R_{50}} k_{ecal}. \tag{9.5}$$

The photon-electron conversion factor, k_{ecal}, is fixed for a given chamber model and is just $k_{R_{50}}$ for an electron beam of arbitrary quality Q_{ecal}, i.e., the value needed, along with P_{gr}^{Q}, to convert $N_{D,w}^{^{60}Co}$ into $N_{D,w}^{Q_{ecal}}$, the absorbed-dose calibration coefficient in an electron beam of quality Q_{ecal}. For TG-51 Q_{ecal} is taken to be a beam with R_{50} = 7.5 cm (Rogers 1998). The electron beam quality conversion factor, $k'_{R_{50}}$, is beam quality dependent and, along with gradient corrections, converts $N_{D,w}^{^{60}Co}$ into $N_{D,w}^{Q}$. In an electron beam, TG-51 gives the dose as:

$$D_w^Q = MP_{gr}^Q k'_{R_{50}} k_{ecal} N_{D,w}^{^{60}Co} \qquad \left[\text{Gy}\right]. \tag{9.6}$$

The photon-electron conversion factor, k_{ecal}, was introduced since: (i) the chamber-to-chamber variation of $k'_{R_{50}}$ is much less than that of $k_{R_{50}}$; (ii) k_{ecal} is a directly measurable quantity based on primary standards for absorbed dose in electron beams; and (iii) k_{ecal} plays a very natural role when cross-calibrating plane-parallel chambers against calibrated cylindrical chambers (see below).

Although the above procedure can be used with plane-parallel chambers, TG-51 strongly encourages users to cross-calibrate them in as high-energy electron beams as available against calibrated cylindrical chambers. This was also recommended by the AAPM's TG-39 on plane-parallel chambers (Almond et al. 1994). The rationale for this at the time was that there had been significant chamber-to-chamber variations reported for plane-parallel chambers in ^{60}Co beams (Kosunen et al. 1994) and there was considerable uncertainty in the calculated values of k_{ecal} due to uncertainties in the measured and the Monte Carlo–calculated values of P_{wall} being used (see section 5.3.2). Since the publication of TG-51 there have been improvements in both the manufacture of these chambers and the measurements and calculations (Kapsch et al. 2007; Mainegra-Hing et al. 2003), but cross-calibration is still preferred until these new chambers and values are being used.

To do a cross-calibration, one determines the beam quality and the reference depth in the high-energy electron beam to be used and measures the responses of the chambers, in sequence, with the point of measurement of both the calibrated cylindrical chamber and the plane-parallel chamber at d_{ref}. While measuring with the cylindrical chamber, P_{gr} is measured (see below). Since the same dose is being measured by the plane-parallel chamber and the cylindrical chamber, by applying equation (9.6) for both chambers, one can deduce that:

$$\left(k_{ecal} N_{D,w}^{^{60}Co}\right)^{pp} = \frac{\left(D_w\right)^{cyl}}{\left(Mk'_{R_{50}}\right)^{pp}} = \frac{\left(MP_{gr} k'_{R_{50}} k_{ecal} N_{D,w}^{^{60}Co}\right)^{cyl}}{\left(Mk'_{R_{50}}\right)^{pp}} \qquad \left[\text{Gy/C}\right]. \tag{9.7}$$

When using the plane-parallel chamber, this value of $\left(k_{ecal}N_{D,w}^{^{60}Co}\right)^{pp}$ is used in equation (9.6), thereby avoiding the need for obtaining the ^{60}Co absorbed-dose calibration coefficient for the plane-parallel chamber. The way in which this equation is developed in terms of k_{ecal} and how the product $\left(k_{ecal}N_{D,w}^{^{60}Co}\right)$ can be naturally used in equation (9.6) are strong reasons for introducing this factor in the first place.

Another major change in TG-51 compared to the TG-21 protocol was that the reference depth for electron beams is at $d_{\text{ref}} = 0.6\,R_{50} - 0.1$ cm instead of at the depth of maximum ionization as in TG-21. As discussed below (see section 4.1.2), this leads to significant simplifications in using stopping-power ratios for realistic electron beams.

2.2 Summary of Relationships Between Quantities in TG-51

The TG-51 formalism introduces several new quantities and it may be useful to review which relationships are defined and which are derived. Equations (9.1), (9.2), (9.4), and (9.5) are the fundamental equations which define the factors $N_{D,w}$, k_Q, $k_{R_{50}}$, $k'_{R_{50}}$, k_{ecal}, and P_{gr}^{Q}. In addition we have, by definition, that:

$$k_{ecal} = k_{R_{50}}^{Q_{ecal}}. \tag{9.8}$$

Starting from these definitions, the dose equations in equation (9.3) for photon beams and equation (9.6) for electron beams can be derived, as can the following general relations which are not used directly in TG-51 but which relate the various absorbed-dose calibration coefficients mentioned, where $N_{D,w}^{Q_{ecal}}$ and $N_{D,w}^{Q}$ are for electron beams:

$$N_{D,w}^{Q_{ecal}} = P_{gr}^{Q_{ecal}} k_{ecal} N_{D,w}^{^{60}Co} \tag{9.9}$$

$$N_{D,w}^{Q} = \frac{P_{gr}^{Q}}{P_{gr}^{Q_{ecal}}} k'^{Q}_{R_{50}} N_{D,w}^{Q_{ecal}}. \tag{9.10}$$

These relationships are summarized in figure 9-1. Equations (9.2), (9.9), and (9.10) can be used to measure k_Q, k_{ecal}, and $k'_{R_{50}}$ by using primary standards to determine absorbed-dose calibration coefficients.

2.3 Rationale for the TG-51 Formalism

The k_Q formalism was not new with TG-51; it had been used for many years in the German protocol for clinical dosimetry (Hohlfeld 1988) and the advantages of this

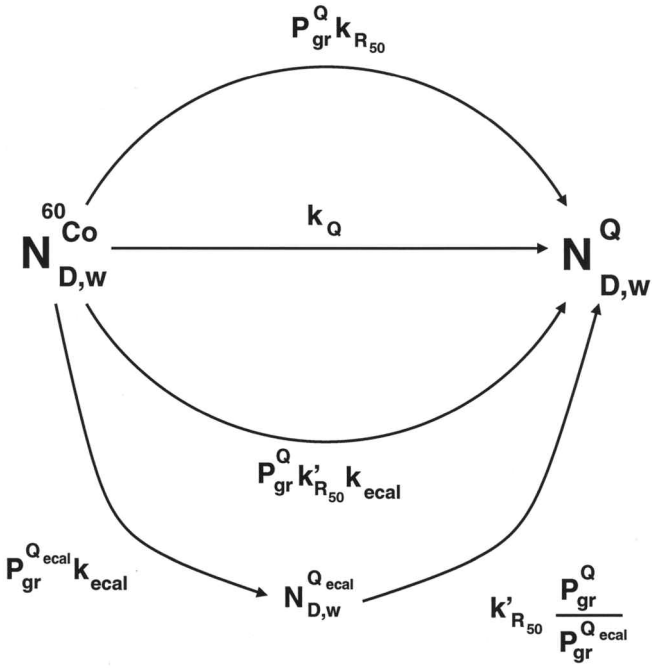

Figure 9-1. Schematic showing relationships between the various absorbed-dose calibration coefficients.

approach had been discussed since the early 1990s (Rogers 1992b, 1996; Andreo 1992; Rogers et al. 1994).

The primary reason for adopting the new approach based on absorbed-dose calibration coefficients is that the resulting protocols and underlying physics are much simpler. This is because the chamber calibration is for the quantity of interest, *viz.,* absorbed dose to water. In contrast, starting from an air-kerma calibration coefficient requires a complex procedure just to get the absorbed dose in a water phantom in a ^{60}Co beam. In addition, the new formalism allows the major factors needed, *viz.,* k_Q, $k'_{R_{50}}$, and k_{ecal}, to be measured directly by using primary standards for absorbed dose. Seuntjens et al. (2000) and others have measured k_Q factors as a function of the beam quality specifier $\%dd(10)_x$ for a wide variety of chambers (see section 8). Similar factors for an air-kerma–based system can also be measured, but the uncertainty on the measurements is considerably higher because those measurements involve two separate primary standards (air kerma and absorbed dose to water) whereas measuring k_Q uses the same primary standard at different beam qualities and hence various uncertainties cancel. Seuntjens et al. (2000) assessed their uncertainties on the k_Q measurements as ±0.4%, whereas the uncertainty on the corresponding air-kerma–based quantities, C_Q, was ±0.6%.

Another reason for using the absorbed-dose based formalism is that calculation of k_Q factors for photon beams are more accurate than the corresponding calculations of C_Q. This is because the k_Q factors are calculated as ratios of corrections, whereas the C_Q factors use the corrections themselves. For example, in the limiting case of ^{60}Co beams, there is no uncertainty on the k_Q value of unity. This argument grows weaker for high-energy photon beams and even weaker in electron beams.

2.4 Fundamentals of Ion Chamber Theory

TG-51 is based on much the same theory of ion chamber response as the TG-21 protocol, but TG-51 does not need to make the conversion from an air-kerma measurement to an absorbed-dose measurement. TG-51 also includes various improvements in the theory of ion chamber response that had been developed in the 15 years since TG-21 was published (e.g., corrections for aluminum electrodes and use of realistic stopping-power ratios in electron beams).

2.4.1 Spencer-Attix Cavity Theory

The central theory underlying ion chamber dosimetry is Spencer-Attix cavity theory (Spencer and Attix 1955), which relates the dose delivered to the gas in the ion chamber, D_{gas}, to the dose in the surrounding medium, D_{med} by the relationship:

$$D_{med} = D_{gas}\left(\frac{\bar{L}}{\rho}\right)_{gas}^{med}, \tag{9.11}$$

where the stopping-power ratio, $\left(\bar{L}/\rho\right)_{gas}^{med}$, is the ratio of the spectrum averaged mass collision stopping powers for the medium to that for the gas where the averaging extends from a minimum energy Δ to the maximum electron energy in the spectrum. The fundamental assumptions of this theory are that: (i) the electron spectrum in the cavity is not changed from the spectrum in the medium; (ii) all the dose in the cavity comes from electrons entering the cavity, i.e., they are not created by photon interactions in the cavity; and (iii) electrons below the energy Δ are in charged particle equilibrium. Unlike Bragg-Gray cavity theory, Spencer-Attix theory applies where charged particle equilibrium above Δ does not exist for the *knock-on* electrons created by electrons. The lack of CPE for knock-ons is generally the case near an interface between media or at the edge of a beam.

The calculation of accurate stopping-power ratios has not changed much since the late 1970s with two exceptions. The stopping-power ratios used by TG-51 for electron beams take into account the realistic nature of the incident electron beams, including the photon contamination, and methods for specifying beam quality have improved. The details regarding the calculated values used in TG-51 are given below in section 4.1.2.

2.4.2 Humidity Effects

To make use of equation (9.11) requires a connection between D_{gas} and the charge measured from the ion chamber. If M is the charge released in the ion chamber (i.e., the corrected charge measurement, see next section), then:

$$D_{gas} = \frac{M}{m_{gas}} \left(\frac{W}{e} \right)_{gas} \qquad \left[\text{Gy} \right], \tag{9.12}$$

where $(W/e)_{gas}$ (in J/C) is the energy deposited in a gas per unit charge of one sign released and m_{gas} is the mass of the gas in the cavity. Fortunately, $(W/e)_{air}$ is generally believed to be a constant for dry air, independent of electron energy (Boutillon and Perroche-Roux 1987) (*viz.,* 33.97±0.05 JC^{-1}, but see section 4.3). One complication in ion chamber dosimetry is that the humidity in the air causes each of the quantities $(W/e)_{gas}$, m_{gas}, and $\left(\bar{L}/\rho\right)_{gas}^{w}$ to vary by up to 1%. This caused considerable confusion in the TG-21 protocol (for a complete discussion see Rogers and Ross (1988) and Mijnheer and Williams (1985) and references therein). The humidity correction factor accounts for these variations:

$$K_h = \left(\frac{W}{e} \right)_{air}^{gas} \frac{m_{air}}{m_{gas}} \left(\frac{\bar{L}}{\rho} \right)_{gas}^{air} . \tag{9.13}$$

Due to offsetting effects and the fact that $\left(\bar{L}/\rho\right)_{gas}^{air}$ is for all practical purposes independent of beam quality, K_h is virtually constant as a function of beam quality and relative humidity, with a value of 0.997 for relative humidity between roughly 15% and 80%. Inserting equation (9.12) into equation (9.11) and rearranging terms leads to:

$$D_{med} = K_h \frac{M}{m_{air}} \left(\frac{W}{e} \right)_{air} \left(\frac{\bar{L}}{\rho} \right)_{air}^{med} = K_h D_{air} \left(\frac{\bar{L}}{\rho} \right)_{air}^{med} , \tag{9.14}$$

where use is made of the fact that $\left(\bar{L}/\rho\right)_{gas}^{med} \left(\bar{L}/\rho\right)_{air}^{gas} = \left(\bar{L}/\rho\right)_{air}^{med}$. All the references are now to dry air, except for M, the charge released. Hence, D_{air} as defined explicitly in equation (9.14) is not strictly the dose to dry air in the chamber because the measured value, M, is still for the humid air. However, one can not define K_h to give a strict dose to dry air, D_{air}, since K_h only actually applies when used in equation (9.14) because it also corrects the stopping-power ratio.

2.4.3 Charge Measurement

In TG-51, the charge released in an ion chamber, M, is given by the fully corrected ion chamber reading:

$$M = P_{ion}P_{tp}P_{elec}P_{pol}M_{raw} \quad \text{[C or rdg]}, \tag{9.15}$$

where M_{raw} is the raw ion chamber reading in coulombs, C, or the instrument's reading units (rdg); P_{tp} is the temperature-pressure correction which corrects the reading to the standard environmental conditions for which the ion chamber's calibration coefficient applies; P_{ion} corrects for incomplete ion collection efficiency; P_{pol} corrects for any polarity effects; and P_{elec} takes into account the electrometer's calibration factor if the electrometer and ion chamber are calibrated separately.

These corrections are well known and discussed in chapter 6 and hence will not be discussed further here except to justify below that the TG-51 recommendation for the ion recombination correction is slightly different from the TG-21 recommendations (see section 6).

2.4.4 Cavity Theory with Corrections

Real ion chambers are not ideal cavities. This raises an issue about the location at which the cavity is measuring the dose, a complex problem, which is discussed below (section 2.4.6). However, for a cylindrical ion chamber, in-phantom calibration coefficients apply with the central axis of the chamber at the point of measurement, and for plane-parallel chambers, the point of measurement is taken as the front of the cavity. There are also several correction factors that are needed before applying equation (9.11), viz.:

$$D_{med} = D_{air}\left(\frac{\bar{L}}{\rho}\right)_{air}^{med} P_{wall}P_{fl}P_{gr}P_{cel}K_h. \tag{9.16}$$

These correction factors are discussed briefly below, but see Alan Nahum's chapter 3 in this monograph for further discussion.

2.4.5 The Wall Correction Factor, P_{wall}

The P_{wall} correction in equation (9.16) accounts for the fact that the wall and other parts of the chamber are not usually made of the same material as the medium. In electron beams, TG-51 takes P_{wall} as unity as is done in TG-21 and other protocols. The values used in photon beams are discussed in section 5.3.1.

2.4.6 The Replacement Correction Factor, $P_{repl} = P_{gr}P_{fl}$

The insertion of a cavity into a medium causes changes in the electron spectrum and the replacement correction factor, P_{repl}, accounts for these changes. P_{repl} can be thought of as having two components: the gradient and fluence correction factors:

$$P_{repl} = P_{gr}P_{fl}. \tag{9.17}$$

The Gradient Correction Factor, P_{gr}. One effect of a cylindrical cavity is, in essence, to move the point of measurement upstream from the center of the chamber. The electron fluence in the cavity is representative of the fluence in the medium at some point closer to the source because there is less attenuation or buildup in the cavity than in the medium. This component of P_{repl} is called the gradient correction, P_{gr}, because its magnitude depends on the dose gradient at the point of measurement. For cylindrical chambers, these corrections depend on the gradient of the dose and on the inner diameter of the ion chamber. The steeper the gradient, the larger the correction. Also, the larger the radius, the larger the correction. For plane-parallel chambers in photon or electron beams, having the point of measurement at the front of the air cavity is already thought to take into account any gradient effects and hence there is no need for a P_{gr} correction, even in regions with a gradient.

For measurements at $d_{\max}$ where the gradient of the dose is zero, P_{gr} is conventionally taken to be 1.00, but for measurements away from $d_{\max}$, P_{gr} becomes important for cylindrical chambers, especially for low-energy electron beams where there are steep gradients. In low-energy beams where the peak of the depth-dose curve is quite sharp, it is not clear that the assumption that P_{gr} is unity is applicable although this is the standard assumption (e.g., in TG-21).

Broadly speaking there are two approaches to handling gradient corrections (aside from making all measurements at $d_{\max}$). A widely used method is to adopt an effective point of measurement that is upstream of the center of the cylindrical ion chamber. One method of establishing how large a shift to use is to compare depth-dose curves measured with cylindrical chambers to those measured with plane-parallel chambers. Based on such measurements by Johansson et al. (1977), the generally accepted (TG-51, TRS-398) offsets are 0.5 r_{cav} for electron beams and 0.6 r_{cav} for photon beams, where r_{cav} is the radius of the cylindrical chamber's cavity. It must be noted that there is a large amount of scatter in the data upon which these offsets are based, and in principle they vary with depth. Nonetheless they are taken as fixed. Work by Sheikh-Bagheri et al. (2000) strongly supported the use of 0.6 r_{cav} for photon beams rather than the TG-21 value of 0.75 r_{cav}.

TG-51 uses the effective point of measurement approach when measuring depth-dose curves for beam quality specification.

The second major approach to handling the gradient correction is to use the central axis of the cylindrical chamber as the point of measurement and then use a multiplicative correction factor. This is the approach adopted by TG-51 for reference dose measurements. In photon beams the correction factor is based on the

work of Cunningham and Sontag (1980) and is discussed more fully in section 5.5. In electron beams the correction factor for cylindrical chambers is measured as:

$$P_{gr} = \frac{M_{raw}\left(d_{\text{ref}} + 0.5 r_{\text{cav}}\right)}{\mathrm{M}_{\text{raw}}\left(d_{\text{ref}}\right)}, \tag{9.18}$$

where M_{raw} is the uncorrected ion chamber reading and the offset (0.5 r_{cav}) was determined as described above. Use of this value of P_{gr} is equivalent to using the effective point of measurement approach. The reason for using equation (9.18) rather than the effective point of measurement approach is that it gives a consistent method that allows for the use of primary standards to provide absorbed-dose calibration coefficients in electron beams since calibration coefficients are traditionally given with the central axis of a cylindrical chamber at the point of measurement. One could define the calibration coefficients to make use of an effective point of measurement, but that presumes knowledge of the correct effective point of measurement. As mentioned above, our knowledge of the offset needed for an effective point of measurement is based on very scattered data. It was felt to be more consistent in the long term to consider explicitly the P_{gr} correction rather than mix it into the calibration of the ion chamber (as done, e.g., in TRS-398 for electron beams).

The Fluence Correction Factor, P_{fl}. The other component of P_{repl} is the fluence correction, P_{fl}, which corrects for other changes in the electron fluence spectrum due to the presence of the cavity.

Fluence corrections are not required for photon beam dose determinations made at or beyond $d_{\max}$ in a broad beam because transient electron equilibrium exists and P_{fl} corrections are only needed if the ion chamber is in a region where full or transient charged particle equilibrium has not been established, i.e., in the build-up region or near the boundaries of a photon beam or anywhere in an electron beam. The Fano theorem tells us that under conditions of charged particle equilibrium the electron spectrum is independent of the density in the medium [see p. 255, Attix (1986)]. To the extent that the cavity gas is just low-density medium material, this theorem tells us that the electron fluence spectrum is not affected by the cavity except in the sense of the gradient correction discussed above, which in essence accounts for there being transient rather complete charged particle equilibrium. Hence no fluence correction factor is needed in regions of transient charged particle equilibrium.

In electron beams there are two competing effects: the in-scatter effect that increases the fluence in the cavity because electrons are not scattered out by the gas ($\Rightarrow P_{fl} < 1.0$) and the obliquity effect which decreases the fluence in the cavity because the electrons go straight instead of scattering ($\Rightarrow P_{fl} > 1.0$). The in-scatter effect tends to dominate, especially at low energies. The value of P_{fl} can be up to 5% less than unity for cylindrical chambers at $d_{\max}$ in electron beams.

Details of P_{fl} values used in TG-51 are discussed in section 5.4.

2.4.7 The Central Electrode Correction Factor, P_{cel}

Cylindrical chambers have central electrodes in their cavities and these have some effect on the chamber response. For electrodes made out of the same material as the phantom, any effect of the electrode can be thought of as part of P_{fl}. Any further effects due to the electrode being made of another material are properly part of P_{wall}. However, it is useful to separate out the correction for electrode effects, and it is called P_{cel}. This correction was ignored in TG-21 but accounted for in TG-51 for aluminum electrodes.

2.5 Derivation of the Equations for Calculating k_Q, $k'_{R_{50}}$, and k_{ecal}

With the fundamental equations of ion chamber theory in place as discussed in the previous section, the equations for the factors used in TG-51 can be derived.

Equation (9.1) for the dose to water in terms of the absorbed-dose calibration coefficient gives:

$$N^Q_{D,w} = \frac{D^Q_w}{M} \qquad \left[\text{Gy/C}\right]. \tag{9.19}$$

Using equation (9.16) for D_w and equation (9.14) to define D_{air} gives:

$$N^Q_{D,w} = \frac{K_h}{m_{air}} \left(\frac{W}{e}\right)_{air} \left(\frac{\bar{L}}{\rho}\right)^w_{air} P_{wall} P_{fl} P_{gr} P_{cel} \qquad \left[\text{Gy/C}\right]. \tag{9.20}$$

Using equation (9.2) to define k_Q, substituting equation (9.20) at the two beam qualities, assuming $(W/e)_{air}$ is constant with beam quality and ignoring the very small variation of K_h with beam quality (Rogers and Ross 1988), one has:

$$k_Q = \frac{\left[\left(\frac{\bar{L}}{\rho}\right)^w_{air} P_{wall} P_{fl} P_{gr} P_{cel}\right]_Q}{\left[\left(\frac{\bar{L}}{\rho}\right)^w_{air} P_{wall} P_{fl} P_{gr} P_{cel}\right]_{^{60}Co}}, \tag{9.21}$$

where the numerator and denominator are evaluated respectively for the beam quality Q of interest and the calibration beam quality, ^{60}Co.

Equation (9.21) applies to both electron and photon beams and was used to calculate the photon beam k_Q factors in TG-51. However, in electron beams, since the factor P_{gr} is not known for an arbitrary value of the beam quality specifier, R_{50}, this equation cannot be used. Instead a measured value of P_{gr} is

used and we can use equation (9.21) and calculate $k_{R_{50}}$ as defined in equation (9.4) as $k_Q \big/ P_{gr}^{Q}$:

$$k_{R_{50}} = \frac{\left[\left(\frac{\bar{L}}{\rho}\right)_{air}^{w} P_{wall} P_{fl} P_{cel}\right]_{Q}}{\left[\left(\frac{\bar{L}}{\rho}\right)_{air}^{w} P_{wall} P_{fl} P_{gr} P_{cel}\right]_{^{60}Co}}. \tag{9.22}$$

Recall that P_{wall} is taken as unity in electron beams in TG-51 but this factor is left here for completeness in view of the discussion in section 5.3.3.

For the reasons discussed above, TG-51 further splits $k_{R_{50}}$ into two components, defined in equation (9.5), *viz.*, k_{ecal} and $k'_{R_{50}}$. Using equation (9.8) for k_{ecal} in terms of $k_{R_{50}}$ and the above equation for $k_{R_{50}}$ gives:

$$k_{ecal} = \frac{\left[\left(\frac{\bar{L}}{\rho}\right)_{air}^{w} P_{wall} P_{fl} P_{cel}\right]_{Q_{ecal}}}{\left[\left(\frac{\bar{L}}{\rho}\right)_{air}^{w} P_{wall} P_{fl} P_{gr} P_{cel}\right]_{^{60}Co}}. \tag{9.23}$$

For a parallel-plate chamber, using the standard assumptions of TG-51 ($P_{gr} = P_{cel} = P_{fl} = 1$ for a plane-parallel chamber and $P_{wall} = 1$ for a plane-parallel chamber in an electron beam) and using the known water to air stopping-power ratios for ^{60}Co (1.1334) and $R_{50} = 7.5$ cm [1.0244, see equation (9.28)] gives:

$$k_{ecal}^{pp} = \frac{0.9038}{P_{wall}^{^{60}Co}}. \tag{9.24}$$

Starting again from equation (9.5) and substituting equation (9.22) and equation (9.23), after lots of cancellation one obtains:

$$k'_{R_{50}} = \frac{\left[\left(\frac{\bar{L}}{\rho}\right)_{air}^{w} P_{wall} P_{fl} P_{cel}\right]_{Q}}{\left[\left(\frac{\bar{L}}{\rho}\right)_{air}^{w} P_{wall} P_{fl} P_{cel}\right]_{Q_{ecal}}}. \tag{9.25}$$

The above equations are the basis of the calculated values in TG-51. After a section to discuss the issue of beam quality specification, and another section describing the basis of the physical data used, the details of the calculations will be described.

3. Beam Quality Specification

To be able to select which values of various quantities should be used in the above equations for k_Q, etc., it is necessary to have good beam quality specifiers in the sense that a given value of the beam quality specifier uniquely determines which value of the quantity to select. The beam quality specifiers used in TG-51, *viz.,* $\%\mathrm{dd}(10)_x$ and R_{50} for photon and electron beams respectively, are different from those used by TG-21 and some other protocols, *viz.,* TPR_{10}^{20} and $\bar{E}_o$.

3.1 Use of $\%\mathrm{dd}(10)_x$ for Photon Beams

The quantity $\%\mathrm{dd}(10)_x$ is the photon component of the photon beam percentage depth-dose at 10 cm depth in a 10×10 cm^2 field on the surface of a water phantom at an SSD of 100 cm. TPR_{10}^{20} is the ratio of the doses measured at constant source-detector distance (SDD) for depths of 20 cm and 10 cm for a 10×10^2 cm field at the point of measurement.

The reason for changing to $\%\mathrm{dd}(10)_x$ for photon beams is that TPR_{10}^{20} was found to be a poor beam quality specifier in the sense that one could have k_Q values for beams of the same value of TPR_{10}^{20} which varied by over 1%, depending on other characteristics of the beam being used either for measurements of k_Q (Seuntjens et al. 2000) or for k_Q calculations (Kosunen and Rogers 1993). Figures 9-2 and 9-3 present calculated stopping-power ratios versus $\%\mathrm{dd}(10)_x$ or TPR_{10}^{20} as the beam quality specifiers. These stopping-power ratios are the dominant component of k_Q and $N_{D,w}$ factors. The fact that there are two groupings of the data in figure 9-2 is why $\%\mathrm{dd}(10)_x$ is considered a better beam quality specifier since there is a single grouping of the data as shown in figure 9-3. If one uses $\%\mathrm{dd}(10)_x$ as the beam quality specifier, both measured and calculated results indicate that for a given value of $\%\mathrm{dd}(10)_x$, there is only one corresponding k_Q value. The choice of $\%\mathrm{dd}(10)_x$ became surprisingly controversial since it was argued that TPR_{10}^{20} is a good beam quality specifier for clinic-like beams and that it is primarily the unfiltered and therefore very soft, nonclinical beams at the National Research Council (NRC) of Canada for which TPR_{10}^{20} is a poor beam quality specifier (Andreo 2000). Figure 9-2 bears this assertion out and proves that TPR_{10}^{20} is a good beam quality specifier for typical commercial, clinical accelerator photon beams available in 2000 (Kalach and Rogers 2003). However, this assertion was a conjecture at the time that TG-51 was being developed. More importantly, up until 1997 the expectation was that TG-51 would be based on an extensive set of k_Q values being measured at NRC. In this case, it would have been mandatory to use $\%\mathrm{dd}(10)_x$ as the beam quality

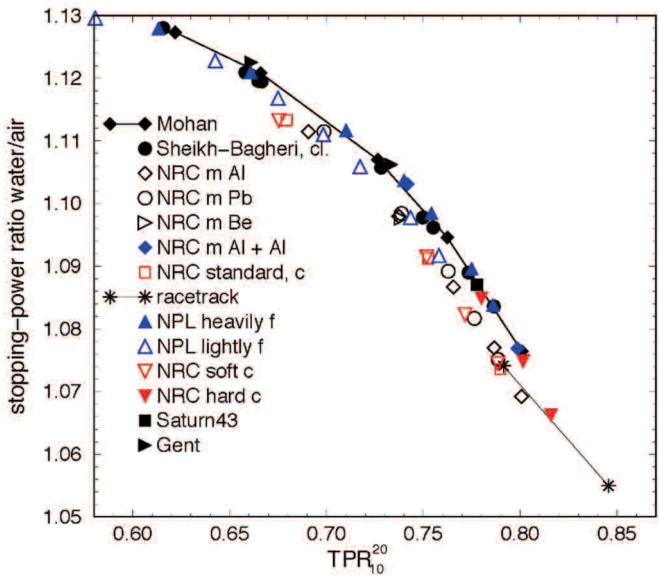

Figure 9-2. Calculated Spencer-Attix water to air stopping-power ratios, which are the dominant component of k_Q and $N_{D,w}$ versus TPR^{20}_{10} for 14 sets of beams. All heavily filtered beams, i.e., clinical and "clinic-like", are shown as closed symbols. (Reprinted from Kalach and Rogers (2003) with permission from American Association of Physicists in Medicine.)

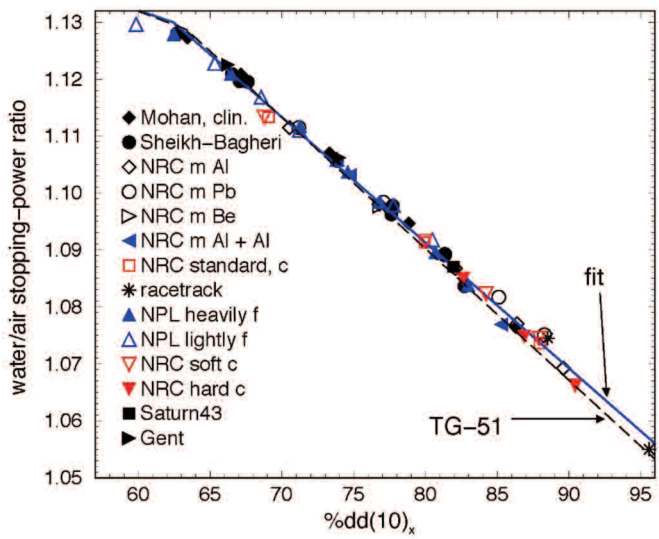

Figure 9-3. Stopping-power ratios as in figure 9-2 except plotted vs. %dd(10)$_x$. The fit, shown as the solid line, is the best fit to these data whereas the long dashed line is the fit (Rogers and Yang 1999) that is used in TG-51 (note that there are two straight lines with the break at 63.4%. (Reprinted from Kalach and Rogers (2003) with permission from American Association of Physicists in Medicine.)

specifier since even the most ardent advocates of using TPR_{10}^{20} recognize that it does not work as a beam quality specifier for the NRC beams.

In the end, the TG-51 protocol is based on calculated values of k_Q but it is still very advantageous to have used $\%\mathrm{dd}(10)_x$ as a beam quality specifier because it has allowed the extensive NRC measured data to be used to validate the calculated values in TG-51, this despite the fact that the lightly filtered NRC beams are distinctly non-clinical. Some of these data from Seuntjens et al. (2000) are reviewed below (see section 8) since they add considerable authority to the values of k_Q presented in TG-51.

With the recent interest in using accelerators without flattening filters because of their advantages in intensity-modulated radiation therapy (IMRT) (Titt et al. 2006), selection of $\%\mathrm{dd}(10)_x$ becomes more valuable since $\%\mathrm{dd}(10)_x$ is still a good beam quality specifier for these very soft beams whereas TPR_{10}^{20} breaks down as a beam quality specifier to select stopping-power ratios by between 0.4% and 1% (Xiong and Rogers 2008).

3.1.1 Correcting for Electron Contamination in Measuring %dd(10)$_x$

All photon beams include electron contamination and thus any measured $\%\mathrm{dd}(10)_\mathrm{m}$ is potentially reduced by this electron contamination if the contamination contributes to the dose at $d_{\max}$, the depth of dose maximum. This complicates the measurement of $\%\mathrm{dd}(10)_x$ which refers only to the photon component of the depth-dose curve.

If the electron contamination were the same for all beams of the same photon beam quality, then one could use $\%\mathrm{dd}(10)_\mathrm{m}$ as the beam quality specifier. Unfortunately this is not the case. However, it has been found that the contribution of electron contamination to the dose at $d_{\max}$ in a 10×10 cm^2 field is negligible for beams with energies of less than about 10 MV. At 10 MV and above, it is necessary to take into account the electron contamination.

If one places a 1 mm slab of lead immediately below an accelerator head, the lead scatters the electrons so broadly that the contribution to the dose at $d_{\max}$ in the phantom is negligible (Li and Rogers 1994; Rogers 1999). However the lead has two further effects: it creates its own electron contamination and it slightly hardens the beam because it preferentially filters out low-energy photons. Fortunately, these two effects can be accurately calculated using Monte Carlo techniques and this allows a simple relationship to be derived between the value of $\%\mathrm{dd}(10)_{\mathrm{Pb}}$, the measured percentage depth-dose (PDD) with the lead foil in place and $\%\mathrm{dd}(10)_x$, the photon component of the PDD of the beam with no lead present. Figure 9-4 presents the Monte Carlo–calculated values of f_e', the ratio of $\%\mathrm{dd}(10)_x$ to $\%\mathrm{dd}(10)_{\mathrm{Pb}}$ for 1 mm lead foils placed 30 or 50 cm from the phantom surface. This figure is the basis of equations (13) and (14) in TG-51 which gives $\%\mathrm{dd}(10)_x$ in the open beam based on the measure value of $\%\mathrm{dd}(10)_{\mathrm{Pb}}$ with the foil in place.

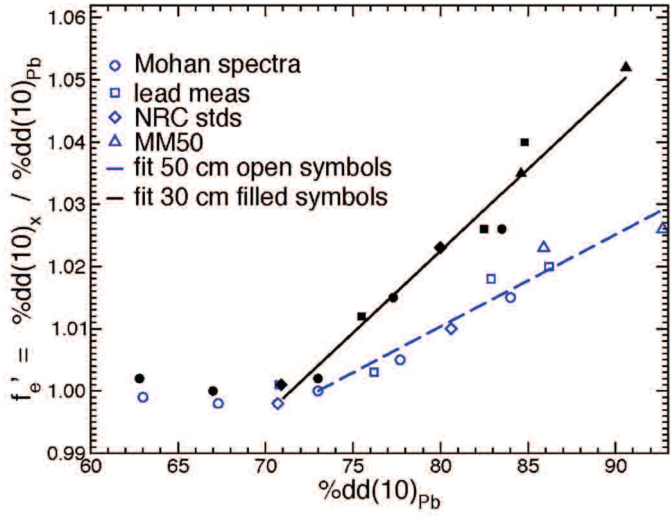

Figure 9-4. Monte Carlo–calculated values of the ratio $f'_e = \%dd(10)_x/\%dd(10)_{Pb}$ as a function of $\%dd(10)_{Pb}$, which is what is measured. The filled symbols are for a 1 mm lead foil placed 30 cm from the phantom surface, and the open symbols are for the foil at 50 cm. (Reprinted from Rogers (1999) with permission from American Association of Physicists in Medicine.)

3.2 Use of R_{50} for Electron Beams

The beam quality specifier for electron beams is the depth at which the dose falls to 50% of its maximum, R_{50}, whereas previously it was $\bar{E}_o$, the mean energy of the electrons at the surface of the phantom (TG-21, TRS-277). This change was not as controversial as the adoption of $\%dd(10)_x$ for photon beams because the values of $\bar{E}_o$ were already indirectly based on values of R_{50}.

The reasons for abandoning $\bar{E}_o$ as a specifier are twofold. The first is that there is no simple way to determine $\bar{E}_o$. Shortly after publication, TG-21's simple $\bar{E}_o = 2.33\ R_{50}$ formula was found to be inaccurate, especially at lower and higher energies (Rogers and Bielajew 1986) and the AAPM's TG-25 report on electron beam dosimetry (Khan et al. 1991) recommended some more accurate formulae, but these were still based on Monte Carlo calculations for monoenergetic electron beams. With the accurate simulation of realistic electron beams it became possible to study the actual values of $\bar{E}_o$ for electron beams (Ding et al. 1996) and these energies do not correlate well with R_{50}. For example, figure 9-5 shows that for 20 MeV beams, the correct mean energy for a 20 MeV Clinac 2100C beam is more than 6% less than predicted by the formula recommended by TG-25. It can be seen

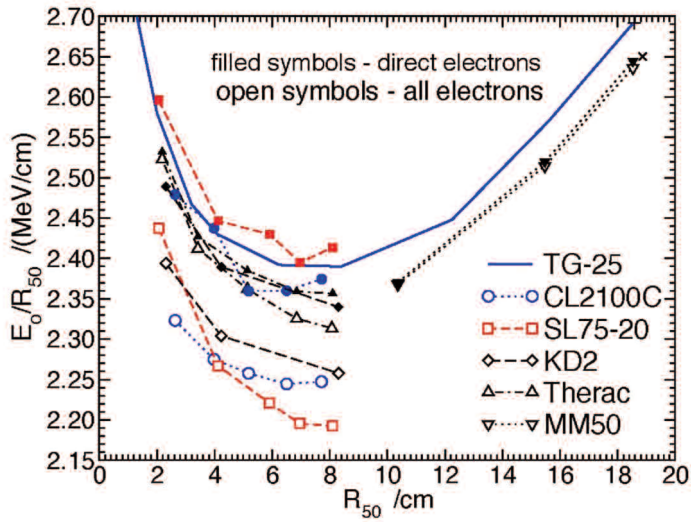

Figure 9-5. Energy-range relationship for broad clinical electron beams as calculated for various realistic beams at an SSD of 100 cm. The open symbols are for all electrons in the field, and filled symbols are for the direct electrons, i.e., excluding those electrons that have interacted with the beam-defining components. $\bar{E}_o$ is the number-averaged mean energy, which is typically up to 1.5% higher than the fluence-averaged mean energy. (Reprinted from Ding et al. (1996) with permission from American Association of Physicists in Medicine.)

that the mean energy of the direct electrons in all of these beams is in better agreement with the formula based on monoenergetic electrons, but even for direct electrons there is a 3% to 4% range in values for a given value of R_{50}.

The second reason for changing to a direct use of R_{50} relates to the fact that stopping-power ratios calculated with realistic instead of mono-energetic electron beams were quite different (see section 4.1.2). David Burns made the astute observation that by going to a new reference depth, one took into account the realistic nature of the electron beams, and got rid of all the fluctuations as well as the need for extensive tables of stopping-power ratios. Burns recommended a reference depth of $d_{\text{ref}} = 0.6\, R_{50} - 0.1$ cm which is at, or very close to $d_{\max}$ for electron beams below about 10 MeV, but is at considerably deeper depths than $d_{\max}$ for higher-energy beams. This reference depth is closely linked to R_{50}, and, as shown in section 4.1.2, the value of $\left(\bar{L}/\rho\right)^{w}_{gas}$ water can be accurately calculated as a function of R_{50}; hence the value of R_{50} is used directly as the beam quality specifier in TG-51.

Moving away from $d_{\max}$ as the reference depth has some disadvantages. It does require an explicit measurement of the gradient correction factor, which is assumed to be unity at $d_{\max}$ in TG-21. However, as discussed above, this assumption is in some doubt anyway. It also requires the use of fluence correction factors away from

d_{max}, despite the fact that the main source of data for these factors is measured at d_{max} (Johansson et al. 1977) (see section 5.4). The final disadvantage, at least for higher-energy beams, is that most clinical patient dose calculation algorithms are based on the dose at d_{max} and thus one must transfer the reference dose at d_{ref} to d_{max}. This leads to some complications, which are discussed below in section 7, but this is not a completely new issue since TRS-277 also allowed reference dosimetry to be done away from d_{max} at 1 or 2 cm depth.

3.2.1 Measuring R_{50}

In TG-21 there was little attention paid to the difference between R_{50} and I_{50}, the depth at which the ionization drops to 50% of its maximum. However there is a systematic difference which can be taken into account as shown by Ding et al. (1995). R_{50} was calculated for many different beams by calculating depth-dose curves using realistic Monte Carlo models of the accelerators and by calculating the water to air stopping-power ratios for those same beams in order to generate depth-ionization curves. These curves were used to extract I_{50}. Figure 9-6 shows the raw data as $R_{50} - I_{50}$ plotted against I_{50} along with a straight-line fit to the data for beams with R_{50} less than about 10 cm, which corresponds to:

$$R_{50} = 1.029\, I_{50} - 0.063 \quad \text{[cm]}. \tag{9.26}$$

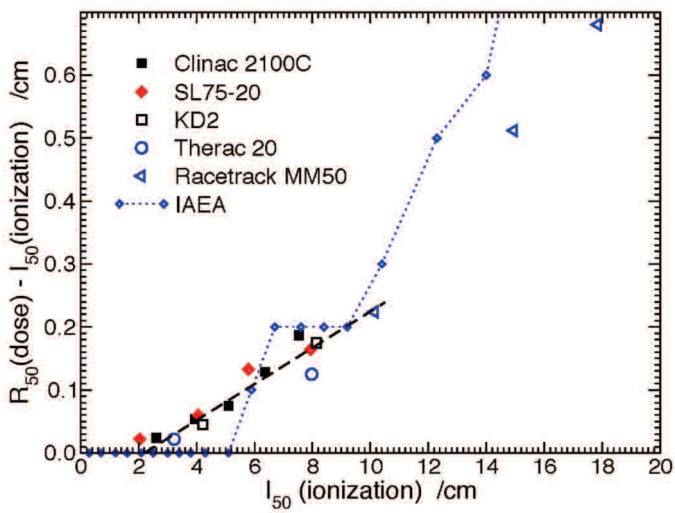

Figure 9-6. Difference between R_{50} and I_{50} as a function of I_{50}. The dashed straight line corresponds to equation (9.26). (Reprinted from Ding et al. (1995) with permission from American Association of Physicists in Medicine.)

This approach assumes that an effective point of measurement is used when the depth-ionization measurements are done (see chapters 7 and 12) and that the product of other corrections, $P_{wall} P_{cel} P_{fl}$, remains constant throughout the depth-dose curve.

Using similar assumptions and the stopping-power ratios for monoenergetic electrons as specified in the report of TG-25 (Khan et al. 1991) to convert measured depth-ionization curves to depth-dose curves, Huq et al. (1997) showed that the above equation was consistent with their measurements within 0.4 mm except for one high-energy beam where it disagreed with experiment by 1.2 mm.

4. The Physical Data Sets in TG-51

TG-51 makes use, either directly or indirectly, of at least three external sets of physical data. In many cases these data are taken directly from previous protocols (TG-21 or TRS-277).

4.1 Stopping Powers and Stopping-Power Ratios

The most critical physical data are electron stopping powers for various materials as these are needed to calculate stopping-power ratios. Since the mid 1980s there has been an agreement amongst primary standards laboratories to use the stopping powers from Intrnational Commission on Radiation Units and Measurements (ICRU) Report 37 (ICRU 1984b) which is based directly on the work of Berger and Seltzer (1983) at National Institute for Standards and Technology (NIST) (then National Bureau of Standards [NBS]). These values have been used consistently in TG-51. This was not the case in TG-21 where the stopping-power ratios for electron beams used this data set, but for photon beams a slightly earlier data set was used from ICRU Report 35 (ICRU 1984a) (also based on NIST data). The differences between these two data sets are considerable.

4.1.1 $\left(\bar{L}/\rho\right)_{air}^{water}$ for Photon Beams

Figure 9-7 compares water to air stopping-power ratios as used in TG-51, TG-21, and TRS-277. For %dd(10)$_x$ values between 75% and 80%, the stopping power used in TG-51 is about 1.3% less than that used in the dose equation for TG-21 although the discrepancy is less for lower-energy beams. TG-21 used a slightly different (0.2% to 0.3% higher) set of values for this same stopping-power ratio when calculating P_{wall} corrections. The data from TRS-277 differ slightly from the TG-51 values only at lower energies. Since most of these data were originally presented as a function of TPR_{10}^{20}, some of the difference could come from the mapping of TPR_{10}^{20} values to %dd(10)$_x$ values (described below in section 5.1).

The stopping-power ratios for photon beams in TG-51 were based on the Monte Carlo–calculated values of $\left(\bar{L}/\rho\right)_{air}^{water}$ and %dd(10)$_x$ for about 25 different realistic

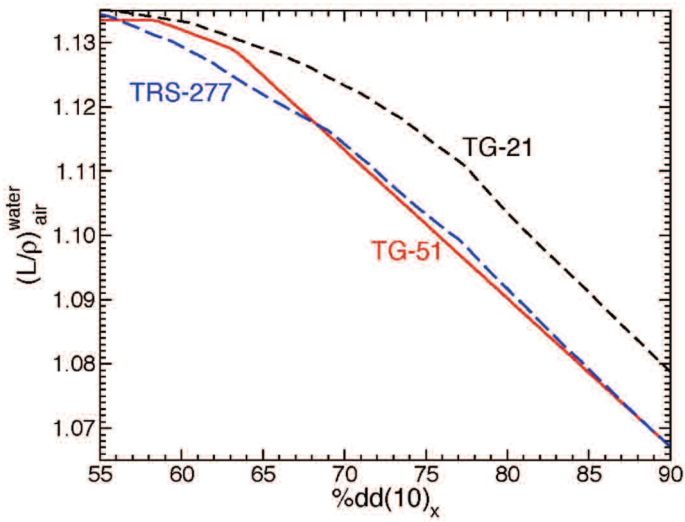

Figure 9-7. Comparison of photon beam Spencer-Attix stopping-power ratios, water to air, at 10 cm depth in 10×10 cm^2 fields of different beam qualities, $\%dd(10)_x$. Tg-51, TRS-277, and TRS-398 values are based on ICRU Report 37 stopping powers and TG-21 values are based on ICRU Report 35 stopping powers.

beam spectra (Rogers and Yang 1999, see figure 9-3 for similar data for about 50 beams). These data are described by:

$$\left(\frac{\bar{L}}{\rho}\right)_{air}^{water} = 1.275 - 0.00231(\%dd(10)_x) \quad (\text{for } \%dd(10)_x \geq 63.35\%). \quad (9.27)$$

The linear fit is used above $\%dd(10)_x = 63.35\%$ and below that a linear interpolation to the ^{60}Co data-point (1.1335 for $\%dd(10)_x = 58.4\%$) is used and for values of $\%dd(10)_x$ below that for ^{60}Co, the ^{60}Co value of the stopping-power ratio is used.

When calculating values of P_{wall}, TG-51 uses values of material to air stopping-power ratios taken from TRS-277. These values are based on stopping powers from ICRU Report 37. The data for a given $\%dd(10)_x$ value are determined by converting $\%dd(10)_x$ values to a TPR_{10}^{20} value using the method described below in section 5.1 and interpolating the data linearly from Tables XIII, XVII, and XX in TRS-277.

4.1.2 $(\bar{L}/\rho)_{air}^{water}$ for Electron Beams

TG-51 takes into account the realistic nature of electron beams when calculating water to air stopping-power ratios, unlike TG-21 and many earlier protocols where stopping-power ratios for monoenergetic electron beams were used. Figure 9-8 shows the effects of using a realistic incident beam calculated using the BEAM Monte Carlo code (Rogers et al. 1995) instead of using a monoenergetic incident

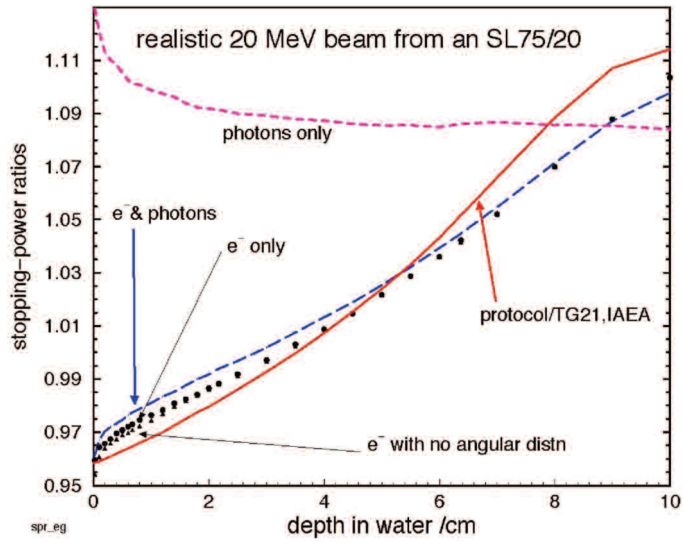

Figure 9-8. Various Monte Carlo–calculated water to air stopping-power ratios vs. depth for a 20 MeV beam from an SL75/20 (a very "dirty" electron beam with R_{50} = 8.1 cm and d_{ref} = 4.8 cm). The solid line represents the stopping-power ratio one would obtain following TG-21, the long dash, that from the complete simulation and the other curves includes only some components of the beam. Based on data in Ding et al. (1995). (Reprinted from Rogers (1999) with permission from American Association of Physicists in Medicine and American Institute of Physics.)

beam. The figure shows that the major effect is from using an electron spectrum. The next most important effect is the inclusion of the photon contamination (Klevenhagen 1994). The angular distribution of the incident beam has only a small effect on the stopping-power ratios.

Figure 9-9 shows the changes caused in the water to air stopping-power ratio at d_{max} for realistic beams compared to the TG-21 values calculated for incident monoenergetic electron beams with the same value of R_{50}. Changes in values calculated with realistic beams vary from a 0.6% decrease for low-energy beams to a 1.2% increase for "dirty" high-energy electron beams. It is possible to use the data in figure 9-9 to correct the procedure used in TG-21 to assign the stopping-power ratio, albeit at the expense of characterizing the beams in terms of $\bar{E}_o$ and the bremsstrahlung tail, D_x, and accepting the relatively large scatter about the fitted line (up to 0.4%). However, as discussed above, Burns' proposal to shift d_{ref} to 0.6 R_{50} – 0.1 cm allows for a much simpler procedure.

Figure 9-10 shows that the required stopping-power ratio can be specified by a single equation, valid only at d_{ref}, *viz.*:

$$\left(\frac{\bar{L}}{\rho}\right)_{air}^{water} = 1.2534 - 0.1487\,(R_{50})^{0.2144}. \qquad (9.28)$$

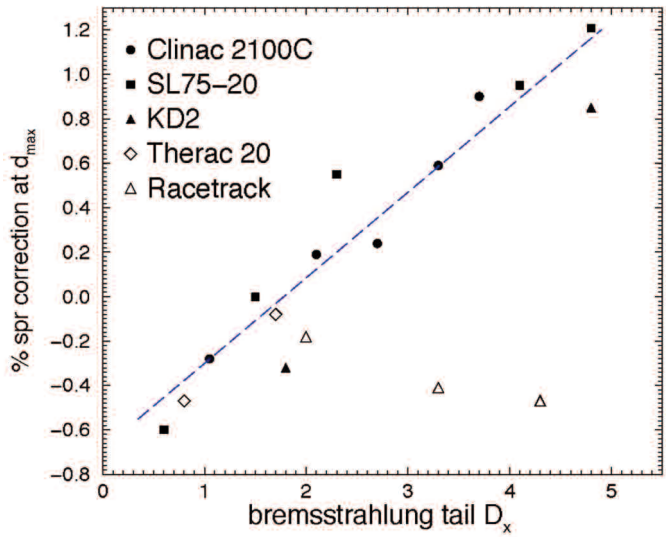

Figure 9-9. The change to the Spencer-Attix water to air stopping-power ratios at d_{max} determined using realistic incident electron beams rather than using the monoenergetic stopping-power ratio data in the AAPM TG-21 protocol and assigning the incident mean energy using $\bar{E}_o = 2.33\ R_{50}$. The correction is given as a function of the bremsstrahlung tail (in %), D_x, taken from Ding et al. (1995).

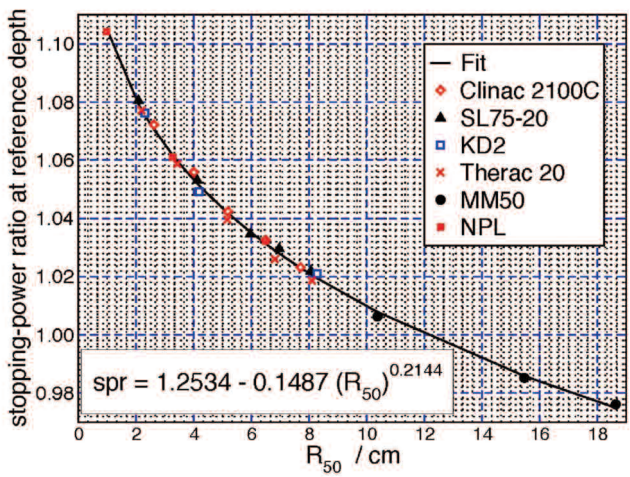

Figure 9-10. Water to air Spencer-Attix mass collision stopping-power ratios at the reference depth $d_{ref} = 0.6\ R_{50} - 0.1$ (cm) fit to $a + bR_{50}^{c}$. The rms deviation is 0.16% and the maximum deviation is 0.26% for the fit given in equation (9.28) (see inset). The stopping-power ratios and R_{50} values are those calculated for realistic beams by Ding et al. (1995). (Reprinted from Burns et al. (1996) with permission from American Association of Physicists in Medicine.)

This equation is used directly in the calculation of various factors in TG-51 and although other parameters may only be accurate for R_{50} greater than 2, this equation is based on a fit to data down to R_{50} = 1.0 cm.

4.1.3 Stopping-Power Ratios: State-of-the-Art

The uncertainties in calculated stopping-power ratios are primarily due to uncertainties in the underlying stopping powers, which mostly depend on a knowledge of the mean ionization value of the materials involved. The ICRU is reevaluating the stopping power data (Steve Seltzer, NIST, private communication, 2008) but it is worth noting that Bichsel and Hiraoka (1992) reported a measured I-value for water of 79.7±0.5 eV compared to the ICRU Report 37's value of 75±3 eV, which is used in the current calculations. However, this 6% change in I-value only leads to changes in water stopping power of between 0.4% at 1 MeV and 0.1% at 10 MeV and thus will not make a significant difference.

Xiong and Rogers (2008) have recently reported new calculations of stopping-power ratios for a variety of clinical beams that differ in several ways from previous calculations. First, they used full accelerator simulations when calculating the stopping-power ratios, which thereby included off-axis variations in both the photon spectra and the photon fluence (horns) unlike prior work which used realistic spectra from point sources. Previously the fluence and the spectrum were considered uniform across the entire field. The accelerator beams considered by Xiong and Rogers also included beams with the flattening filters removed because there are suggestions that this is more efficient when doing IMRT treatments (Titt et al. 2006). Despite the variations in the beams, the underlying relationship between $\left(\bar{L}/\rho\right)_{air}^{water}$ and $\%\mathrm{dd}(10)_x$ remains valid as used in TG-51 although a slight change would improve the relationship marginally if the protocol were to be rewritten.

4.2 Mass-Energy Absorption Coefficients

The ratio of mass-energy absorption coefficients for material A to material B, $\left(\overline{\mu_{en}}/\rho\right)_B^A$, plays a role in dosimetry since it relates the doses in two materials in a photon beam when there is charged particle equilibrium (which rarely occurs for small volumes in high-energy beams). These ratios play a minor role in TG-51 since they are needed to calculate ratios of P_{wall} values in equation (9.21) using equation (9.33) presented below for P_{wall}. Thus they are not as important as in TG-21 where they are used directly in the equation for N_{gas} in addition to the calculation of P_{wall} (not its ratio) and K_{comp}. The values of ratios of mass-energy absorption coefficients in TG-51 are taken directly from TRS-277. These values were calculated for a point at depth in a phantom by Cunningham using the Monte Carlo techniques described in an earlier paper by Cunningham et al. (1986). The basic mass energy absorption coefficient data are from Hubbell (1982). In contrast, the ratios of mass-energy absorption coefficients in TG-21 are based on a more

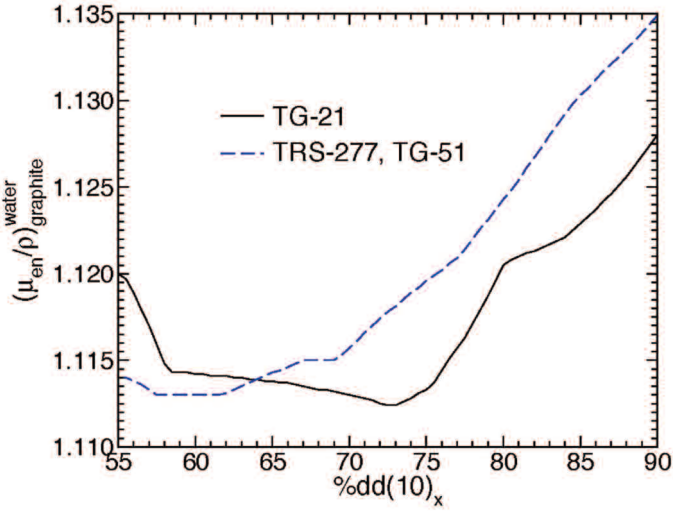

Figure 9-11. Ratio of spectrum averaged mass-energy absorption coefficients, water to graphite as used in TRS-277 and TG-51, compared to the values used in TG-21 for P_{wall} calculations.

restricted set of analytic calculations (Cunningham and Schulz 1984) which did not include scattered photons and which were based on the mass-energy absorption coefficient data of Howerton (as quoted in Johns and Cunningham 1983). These two data sets are compared in figure 9-11, which shows up to 1% changes in the ratios for water to graphite.

4.2.1 Mass-Energy Absorption Coefficients: State-of-the-Art

There has been little investigation of ratios of mass-energy absorption coefficients. However, in a paper about P_{wall} values, Buckley and Rogers (2006b) calculated a wide range of these ratios in an attempt to explain some P_{wall} differences, which are discussed below (see section 5.3.3). The results showed that the values used in TG-51 are within ≈0.1% usually, and at worst 0.3%, of the values calculated with an EGSnrc Monte Carlo calculation at depth in a phantom using the latest values of photon cross sections and realistic accelerator spectra.

4.3 $(W/e)_{air}$

TG-51 is independent of the actual value of the mean energy deposited by electrons slowing down per coulomb of charge of one sign released in air, but it does depend on the value of $(W/e)_{air}$ being a constant over the entire range of beam qualities considered here. The evidence for this constancy is not very strong. In fact, Svensson and Brahme (1986) reanalyzed an extensive set of data measured by Domen

and Lamperti (1976) and concluded that (W/e) varies by about 1%. The situation is complex to assess, and an analysis including the effects of realistic electron beams in the experiment could change the situation further. Nonetheless, the assumption continues to be made that the value of (W/e) does not change. As we shall see below, the good agreement between the measured and calculated values of k_Q suggests that any variation of (W/e) in photon beams is not too important.

For comparisons to the air-kerma–based protocols such as TG-21, one needs a value of $(W/e)_{air}$. This value was reviewed in ICRU Report 31 (ICRU 1979) but the standard value today is taken from the work of Boutillon and Perroche-Roux (1987). They reanalyzed all the previous data, took into account correlations and came up with a value for dry air of $(W/e)_{air} = 33.97 \pm 0.06$ J/C.

4.3.1 $(W/e)_{air}$: State-of-the-Art

The subject of the determination of a value for $(W/e)_{air}$ is very complex since it requires knowledge of the value of $\left(\bar{L}/\rho\right)_{air}^{graphite}$. However, for the comparison mentioned in the previous paragraph, one only needs a knowledge of the product of these two quantities, *viz.*, $\left(W/e\right)_{air}\left(\bar{L}/\rho\right)_{air}^{graphite}$ in a ^{60}Co beam. There are strong indications that the accepted value of this product is actually wrong by about 1%, which means that most primary standards for air kerma will require a 1% reduction (Wang and Rogers 2008b). While not directly relevant to TG-51 except for the comparisons mentioned above, this volatility in primary standards for air kerma in a ^{60}Co beam is yet another strong reason for the TG-51 change to using calibration coefficients based on primary standards for absorbed dose to water, which have not been so volatile.

5. Calculation of TG-51 Factors

The factors k_Q, k_{ecal}, and $k'_{R_{50}}$ are needed in TG-51 for all reference ion chambers as a function of beam quality. These are calculated using equations (9.21), (9.23), and (9.25), respectively. These equations make use of the various factors defined and discussed in the above sections, *viz.*, $\left(\bar{L}/\rho\right)_{air}^{water}$, P_{wall}, P_{fl}, P_{gr}, and P_{cel}. In the following sections, the details of the calculations for each factor are reviewed in turn and, where appropriate, compared to those in TG-21.

The calculations for TG-51 were done by a suite of programs called PROT (Rogers and Booth 2009). A detailed report describing this suite of programs will be available on-line at http://www.physics.carleton.ca/~drogers/pubs/papers/.

5.1 Converting between $\%dd(10)_x$ and TPR_{10}^{20}

TG-51 uses various values from TRS-277 which are presented as a function of TPR_{10}^{20}. It is thus necessary to convert between the two beam qualities. This was

done by using a set of TPR_{10}^{20} values (Kosunen and Rogers 1993) and $\%dd(10)_x$ values for the same nine clinical or clinic-like spectra (Rogers and Yang 1999). These pairs of values have been fit by cubic polynomials to give:

$$\%dd\left(10\right)_x = -106.6 + 759.3 \times TPR_{10}^{20} - 1256. \times \left(TPR_{10}^{20}\right)^2 + 756.8 \times \left(TPR_{10}^{20}\right)^3 \quad (9.29)$$

and

$$TPR_{10}^{20} = -2.079 + 0.08732 \times \%dd(10)_x - 0.0009132 \times (\%dd(10)_x)^2 + 3.348 \times 10^{-6} \times (\%dd(10)_x)^3 \quad (9.30)$$

These relationships do not hold in general in nature. If there were a one-to-one correspondence for all beams, as implied by the equations, there would be no point in using $\%dd(10)_x$ instead of TPR_{10}^{20}. However, these relationships were considered accurate enough for the purposes of converting between beam quality specifiers for clinical beams to allow access to physical data such as mass-energy absorption coefficients, which were tabulated in terms of TPR_{10}^{20} when they are needed for calculations of corrections such as P_{wall}.

5.1.1 Converting Between %dd(10)$_x$ and TPR_{10}^{20}: State-of-the-Art

Since TG-51 was produced, Kalach and Rogers (2003) did a much more detailed study of the relationship between $\%dd(10)_x$ and TPR_{10}^{20} and found that for a very broad range of clinical and clinic-like beams (i.e., heavily filtered beams), there is a unique relationship between $\%dd(10)_x$ and TPR_{10}^{20}, *viz.*:

$$TPR_{10}^{20} = -0.8228 + 0.0342\ (\%dd(10)_x) - 0.0001776\ (\%dd(10)_x)^2, \quad (9.31)$$

with an rms deviation of the TPR_{10}^{20} data about the fit of 0.0034 and a maximum deviation of 0.007. In the other direction one has:

$$\%dd\left(10\right)_x = -430.62 + 2181.9\left(TPR_{10}^{20}\right) - 3318.3\left(TPR_{10}^{20}\right)^2 + 1746.5\left(TPR_{10}^{20}\right)^3 \quad (9.32)$$

The rms deviation is 0.46 and the maximum deviation in values of $\%dd(10)_x$ from the fit is 0.9%.

For heavily filtered beams, these expressions can be used to check measured values of TPR_{10}^{20} and $\%dd(10)_x$ and ensure that they are consistent.

Figure 9-12 compares the results from that study to those developed and used in the calculations for TG-51. The two fitted curves are in excellent agreement. The fit to the measured data is also in good agreement with the fit to the calculated data, although there is considerable scatter in the measured results [see original paper, Kalach and Rogers (2003)].

Note that these relationships do not apply for lightly filtered beams either in standards labs or for IMRT machines without flattening filters.

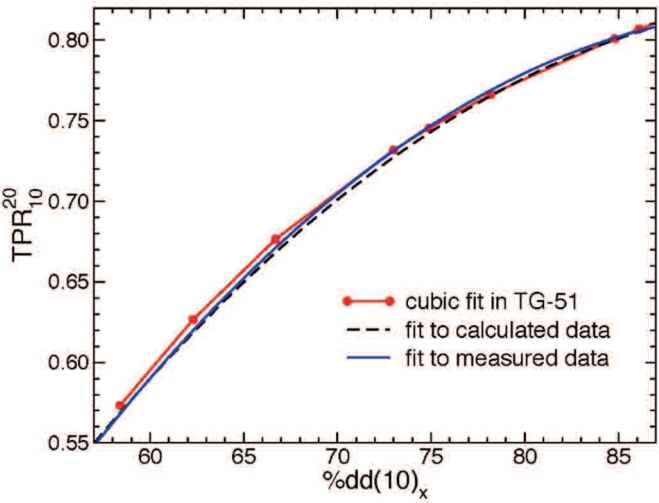

Figure 9-12. Fits to various sets of TPR_{10}^{20} and $\%dd(10)_x$ data. The line with circles is the fit used in TG-51 to go from $\%dd(10)_x$ to TPR_{10}^{20} [equation (9.30)]. The solid line is a quadratic fit [equation (9.31)] to the calculated data and the dashed line is a fit to the measured data in Kalach and Rogers (2003).

5.2 The Central Electrode Correction Factor, P_{cel}

As discussed in section 2.4.7, the central electrode correction takes into account the effects of the central electrode on the chamber response, although traditionally one does not take them into account if they are of the same material as the wall.

Many chambers have aluminum electrodes to give a flat energy response in low-energy x-ray fields (e.g., many NE and PTW chambers). These aluminum electrodes have a distinct effect on the response even in high-energy photon beams. Although the value of P_{cel} is close to unity in electron beams, the effect of TG-51 accounting for P_{cel} is actually larger in electron beams than in photon beams because the final dose determination includes the factor $P_{cel}(e^-)/P_{cel}(^{60}Co)$ and the factor in the denominator is quite large (see below). In contrast, the equivalent ratio for photon beams is closer to unity.

Ma and Nahum (1993) used Monte Carlo techniques to calculate that a 1 mm diameter aluminum electrode increases chamber response in photon beams by 0.4% to 0.8% relative to a graphite electrode, requiring a P_{cel} correction factor less than unity (see table 9-1), as shown in figure 9-13 along with the linear fit as a function of $\%dd(10)_x$ used in TG-51. The measured data of Palm and Mattsson (1999) are also shown and are in quite good agreement with the calculations.

The effect of an aluminum electrode in electron beams is quite small and varies with depth. The results of Ma and Nahum indicate that P_{cel} at d_{ref} is unity up to 13 MeV

Table 9-1. P_{cel} Correction Factor Required for Farmer Chambers with an Aluminum Electrode of 1 mm Diameter, Based on the Calculations of Ma and Nahum (1993).

Factors apply past d_{max} in photon beams and near d_{max} or 0.6 R_{50} – 0.1 cm in electron beams. The %dd(10)$_x$ values exclude electron contamination. Note that P_{cel} as defined here is consistent with the other correction factors but is not the same as the P_{cel} correction in TRS-277.

		Beam Quality	
NAP/MeV	**TPR_{10}^{20}**	**%dd(10)$_x$**	**P_{cel}**
Photons			
^{60}Co	0.58	56%	0.9926(15)
4 MV	0.62	62%	0.9935(7)
6 MV	0.67	67%	0.9930(11)
10 MV	0.73	72%	0.9945(9)
15 MV	0.76	78%	0.9955(16)
24 MV	0.80	86%	0.9957(9)
Electrons			
<13 MeV			1.000
≥13 MeV			0.998

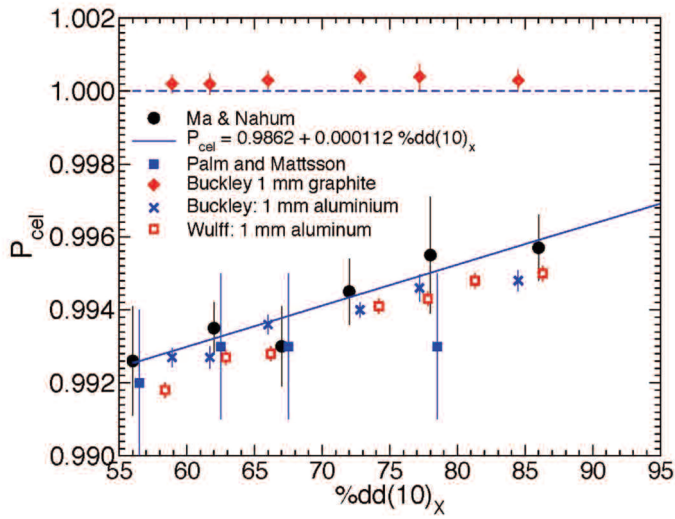

Figure 9-13. Values of P_{cel} for photon beams as calculated by Ma and Nahum (1993) and measured by Palm and Mattsson (1999). The solid line is the fit used in TG-51 to the data of Ma and Nahum. The more recent and much higher precision values of Buckley et al. (2004) and Wulff et al. (2008a) are seen to be in good agreement with the older values.

and about 0.998 at 20 MeV (for monoenergetic incident beams). The experimental data of Palm and Mattsson (1999) are in agreement with the calculations within the uncertainties of about 0.2%. Originally this correction was to be implemented in TG-51 as 1.00 up to 13 MeV and 0.998 above that energy. This led to a 0.2% discontinuity in calculated $k'_{R_{50}}$ values at R_{50} = 5.5 cm (Rogers 1998). To get rid of this discontinuity, TG-51 treats P_{cel} as 1.0 for $R_{50} < 4.3$ cm, 0.998 for $R_{50} > 6.7$ cm and linearly interpolates on R_{50} between these values as shown in figure 9-14.

5.2.1 P_{cel}: State-of-the-Art

Buckley et al. (2004) did an extensive study of the electrode effect under reference conditions in electron and photon beams. Results from that work have already been seen in figures 9-13 and 9-14. Wulff et al. (2008b) have also calculated P_{cel} values, which are shown in the figure. In the photon beam case both sets of new results have much higher statistical precision but agree well with the values used in TG-51. The photon beam results also confirm that a graphite electrode has a negligible effect and thus it does not matter whether it is considered or not.

In electron beams the newer results show some small differences with the previous results. In particular a 1 mm aluminum electrode would appear to require P_{cel} = 0.999 in all beams. Perhaps more interestingly, figure 9-14 indicates that a graphite electrode requires a correction which is between 0.1% and 0.2% greater than unity. Fortunately these differences from TG-51 are not very significant.

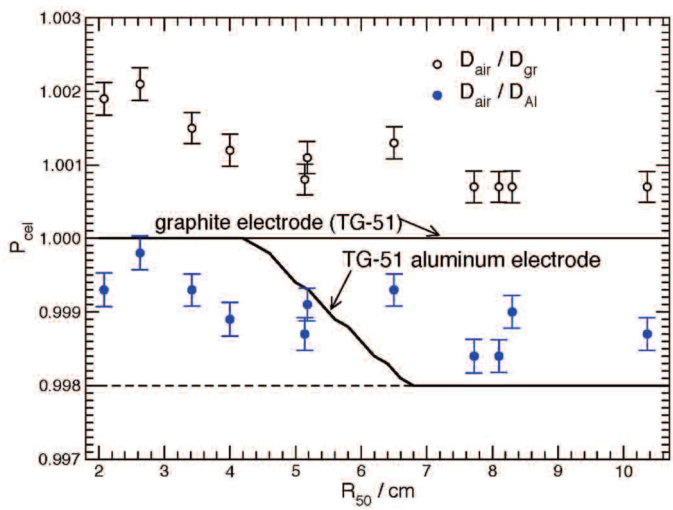

Figure 9-14. Monte Carlo–calculated values of P_{cel} for electron beams compared to the values in TG-51. The TG-51 values were based on a few calculated values by Ma and Nahum (1993) interpolated for depth whereas the Buckley et al. results are for d_{ref} and realistic beams. [Reproduced from Buckley et al. (2004) with permission from American Association of Physicists in Medicine.]

Wulff et al. (2008a) have repeated some of the calculations of Buckley et al. (2004) and get close agreement. They also did the calculations as a function of depth in a 6 MV beam and found that P_{cel} was constant. More interestingly they showed that the on-axis value of P_{cel} decreased by 0.3% in a 40×40 cm^2 field compared to the reference field of 10×10 cm^2 and showed that it decreased by another 1% as the ion chamber passed through the penumbra of the 6 MV field.

5.3 The Wall Correction Factor, P_{wall}

5.3.1 P_{wall} for Cylindrical Chambers

In electron beams, P_{wall} was commonly assumed to be 1.00 and TG-51 (and TRS-398) continued to assume this although it is known to be a poor assumption. Nahum (1988) presented a theoretical model of the effect of the wall material on the electron spectrum in the cavity (see chapter 3). It qualitatively agrees with the experimental data in an extreme case. Based on this model, Nahum has shown that the wall effect in electron beams due to changes in the spectrum, should be less than 1%, and usually much less for situations of importance in clinical dosimetry.

In photon beams, the correction factor for the wall effect for cylindrical chambers was initially given by Almond and Svensson (1977). This has been slightly extended (Hanson and Tinoco 1985; Gillin et al. 1985) to handle the case of a waterproofing sheath as well as the wall:

$$P_{wall} = \frac{\alpha\left(\frac{\bar{L}}{\rho}\right)_{air}^{wall}\left(\frac{\overline{\mu_{en}}}{\rho}\right)_{wall}^{med} + \tau\left(\frac{\bar{L}}{\rho}\right)_{air}^{sheath}\left(\frac{\overline{\mu_{en}}}{\rho}\right)_{sheath}^{med} + (1-\alpha-\tau)\left(\frac{\bar{L}}{\rho}\right)_{air}^{med}}{\left(\frac{\bar{L}}{\rho}\right)_{air}^{med}}, \tag{9.33}$$

where $\left(\overline{\mu_{en}}/\rho\right)_B^A$ is the ratio of mass energy absorption coefficients; α is the fraction of ionization in the cavity due to electrons originating in the chamber wall; τ is the fraction of ionization in the cavity due to electrons originating in the waterproofing sheath and $(1 - \alpha - \tau)$ is the fraction due to electrons originating in the phantom.

There is another formula for P_{wall} that was originally developed by Shiragai (1978, 1979) and extended to the sheath case by analogy to equation (9.33):

$$P_{wall} = \frac{1}{\left(\frac{\bar{L}}{\rho}\right)_{air}^{med}\left[\alpha\left(\frac{\bar{L}}{\rho}\right)_{wall}^{air}\left(\frac{\overline{\mu_{en}}}{\rho}\right)_{med}^{wall} + \tau\left(\frac{\bar{L}}{\rho}\right)_{sheath}^{air}\left(\frac{\overline{\mu_{en}}}{\rho}\right)_{med}^{sheath} + (1-\alpha-\tau)\left(\frac{\bar{L}}{\rho}\right)_{med}^{air}\right]}. \tag{9.34}$$

This formula is on a more solid theoretical foundation. However, it turns out that these equations produce virtually identical numerical results. For 0.05 g/cm^2 thick walls, the two equations give P_{wall} values within 0.01% for graphite and 0.02% for A-150 walls (Rogers 1991; Rogers and Booth 2009). TG-51 has consistently used equation (9.33).

The P_{wall} correction is typically 1% or less for most ion chambers, but the accuracy of the formula has not been rigorously demonstrated and there were indications that there are problems with it (Hanson and Tinoco 1985; Gillin et al. 1985; Ross et al. 1994). Also, there are conceptual problems with the P_{wall} factor since it uses many approximations in its derivation and it ignores changes in attenuation and scatter by the wall. For a more complete discussion and derivation of the P_{wall} equation [equation (9.34)], see Rogers (1992c) or Nahum (1994).

To calculate P_{wall} in photon beams one must know values of α and possibly τ and the values used in TG-51 are shown in figure 9-15. These quantities are thought to be relatively independent of the material involved and are given as a function of wall thickness in g/cm^2. The values needed are determined from the wall and sheath thickness respectively by interpolating tabulated values based on figures 1 and 7 of TG-21 after converting the beam quality specifier, $\%dd(10)_x$ to TPR_{10}^{20} using equation (9.30) and then using Figure 3 in TG-21 to convert TPR_{10}^{20} into nominal accel-

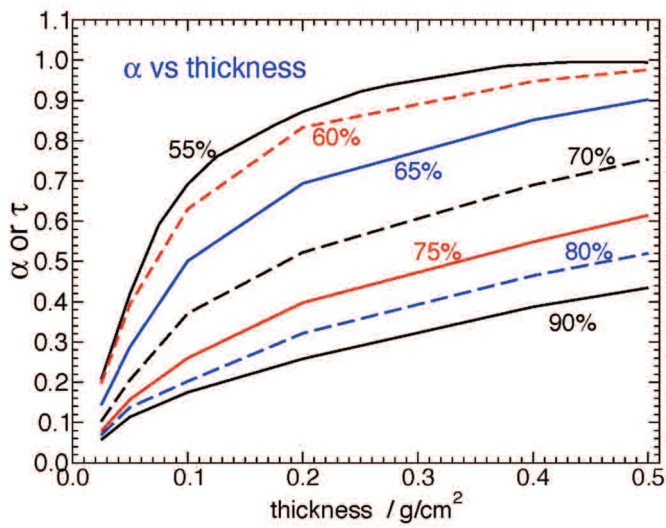

Figure 9-15. The values of α or τ as a function of wall thickness with beam quality specified in terms of $\%dd(10)_x$ as used in TG-51 calculations of P_{wall}. Data are based on interpolations of Figures 1 and 7 of TG-21. For values when walls are less than 0.05 g/cm^2, the thinnest value in the original figure, TG-51 uses linear interpolation to 0.0 for zero wall thickness. Values of α and τ are assumed independent of the material of the wall.

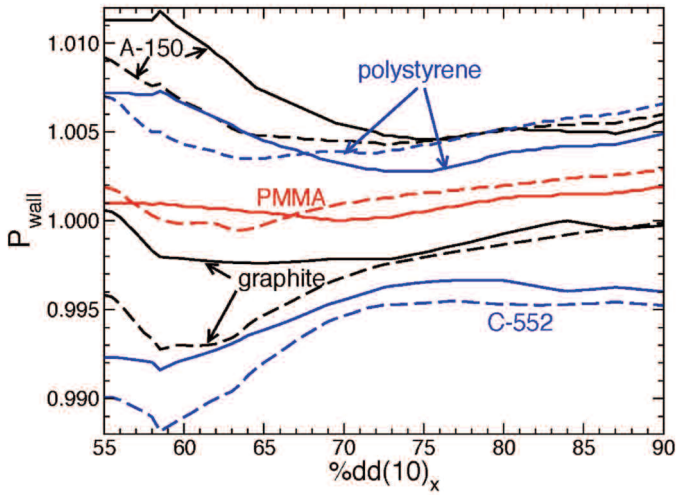

Figure 9-16. Comparison of P_{wall} values for 0.05 g/cm^2 walls of different materials as calculated for TG-51 (dashed lines) vs. the value calculated using TG-21 (solid lines). The differences are entirely due to changes in the data sets.

erating potential (NAP) in MV before interpolating the original figures. Buckley et al. (2003) did a series of Monte Carlo calculations of α for a ^{60}Co beam and showed that the correct values can be as much as 15% different from the values used in TG-51 and that the linear interpolation to zero wall thickness is not ideal. However, given the complete breakdown of the P_{wall} formalism [i.e., equation (9.33)] reported in Buckley and Rogers (2006b) (see section 5.3.3), the issue of accurate values of α has not been pursued.

The other data needed to calculate P_{wall} values in TG-51 are stopping-power ratios and mass-energy absorption coefficients. Their sources are described above in sections 4.1 and 4.2.

Figure 9-16 compares the values of P_{wall} for chambers of different wall materials with a thickness of 0.05 g/cm^2 as calculated in TG-51 and TG-21 protocols.

5.3.2 P_{wall} for Plane-Parallel Chambers

The above formulation applies to cylindrical chambers. For plane-parallel chambers the P_{wall} correction in a ^{60}Co beam is needed in equation (9.24) for the calculation of k_{ecal} to account for the effects of the chamber wall materials being different from the material of the phantom. Equation (9.33) cannot be applied since the values of α and τ are not known, and, more importantly, there are major effects due to variations in backscatter from the insulator at the back of the chamber (Rogers 1992a) and these are not accounted for in the formula. TG-51 has based its values of P_{wall} for plane-parallel chambers on values calculated with the EGS4 Monte

Carlo code although these calculations were known to be subject to large systematic uncertainties (about ±1%) and rely on having an accurate description of the chamber (Rogers 1992a; 1998). There are also measured data available (Laitano et al. 1993; Ding and Cygler 1998; Palm et al. 2000; Araki et al. 2000). The measured values were known to be subject to large uncertainties since they require either knowledge of, or assumptions about, various other correction factors such as P_{repl}.

When TG-51 was being developed, for photon beam energies other than ^{60}Co there were no values of P_{wall} that were considered complete enough or reliable enough to allow use of plane-parallel chambers in accelerator photon beams and thus they were excluded from photon beam dosimetry.

In electron beams, although TG-51 takes P_{wall} = 1.00 for plane-parallel chambers (as it does for cylindrical chambers) several authors (Klevenhagen 1991; Hunt et al. 1988) have pointed out that for plane-parallel chambers, the electron backscatter from non-water materials behind the air cavity is different from that of water and this induces a change in the ion chamber reading. In principle this could have been corrected for using the P_{wall} corrections given in table 9-2. The corrections can be substantial for low-energy beams. Preliminary results of Monte Carlo calculations of this effect for the entire chamber for NACP and PTW/Markus chambers also indicated an effect of the order of 1% or 2% (Ma and Rogers 1995). Nonetheless this factor was taken as 1.0 in TG-51 (and TRS-398) due to the incomplete data available at that time.

5.3.3 P_{wall}: State-of-the-Art

There has been considerable work on the P_{wall} correction since TG-51 was published.

P_{wall} Values for Plane-Parallel Chambers in ^{60}Co. Since there were known systematic uncertainties that were the basis for the P_{wall} values for plane-parallel

Table 9-2. Electron Beam P_{wall} Correction Factor for Plane-Parallel Chambers with Effectively Thick Back Walls of the Materials Shown

Data from Klevenhagen (1991), based on the results of Hunt et al. (1988).

E_z, energy at depth of chamber (MeV)	Graphite	PMMA	Polystyrene
3	1.010	1.012	1.021
4	1.009	1.011	1.018
6	1.006	1.008	1.013
10	1.004	1.005	1.009
14	1.003	1.003	1.006
20	1.001	1.001	1.002

chambers used to calculate the values of k_{ecal} using equation (9.24), Mainegra-Hing et al. (2003) redid these calculations using EGSnrc which calculates ion chamber response much more accurately than EGS4 (Kawrakow 2000). Figure 9-17 shows that this systematically increased the values of P_{wall} and hence k_{ecal}. The new calculations improved agreement with experiment although all of the experimental methods required values of parameters such as P_{wall} and P_{cel} for cylindrical and plane-parallel chambers in high-energy beams and, as we will see below, there have been significant changes in many of these values, thereby implying changes in the experimental results.

Mainegra-Hing et al. (2003) showed that the uncertainties on the calculated values of P_{wall} from the 1% uncertainties on the underlying photon cross sections is typically 0.3%. Thus the uncertainties on the calculated values are likely smaller than the measurement uncertainties on the condition that the descriptions of the ion chambers are accurate. Recent work (Dohm et al. 2001; Christ et al 2002; Kapsch et al. 2007) suggests that the chamber to chamber variations with parallel plate chambers are much better, at least with the Roos, Advanced Markus and Markus chambers, than reported for the NACP chambers by Kosunen et al. (1994). Once it is clearly established that plane-parallel chambers are consistent from chamber to

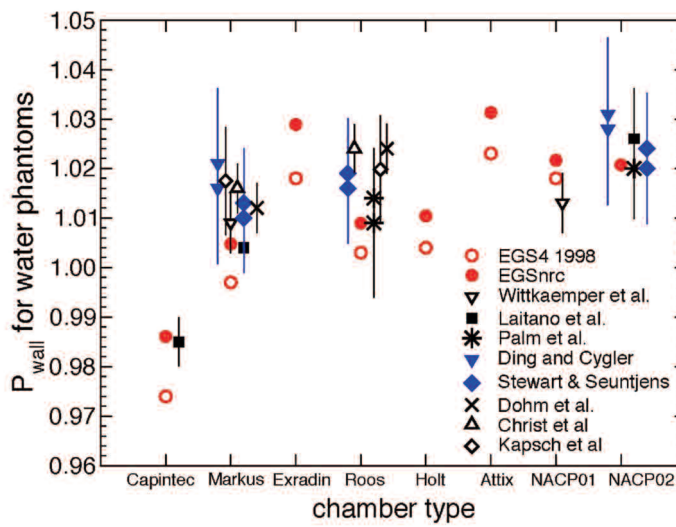

Figure 9-17. A comparison of the values of P_{wall} used in TG-51 [EGS4 calculations (Rogers 1998)] to the more recent EGSnrc calculations of Mainegra-Hing et al. (2003) and to a variety of experimental determinations. For complete references for the experimental work, see Mainegra-Hing et al. (2003) and Kapsch et al. (2007). Several authors used two methods to analyze their measurements and both results are shown. Figure is redrawn from Mainegra-Hing et al. (2003) with extra data from Kapsch et al. (2007). (Redrawn with permission from American Association of Physicists in Medicine.)

chamber, then the values of k_{ecal} can be trusted (either calculated or measured). This means that plane-parallel chambers calibrated directly in ^{60}Co beams will be a reasonable alternative despite the fact that TG-51 strongly encouraged the use of the cross-calibration technique.

P_{wall} Values for Cylindrical Chambers in Photon Beams. Buckley and Rogers (2006b) did a detailed study of Monte Carlo calculated values of P_{wall} under reference conditions (i.e., at 10 cm depth in a 10×10 cm^2 photon beam). In that study they demonstrated that their calculated values led to much better agreement with three different previously reported measurements than when P_{wall} values calculated with equation (9.33) were used. Figure 9-18 presents the ratios of the Monte Carlo calculated values to those used in TG-51, and for wall materials such as graphite and A150 (tissue equivalent plastic) the differences are up to 0.8%. It was shown that the differences were due to the breakdown of equation (9.33) because the values of all the physical parameters used in the equation were calculated with the same cross sections as used in the Monte Carlo calculations and this did not significantly change the P_{wall} values using equation (9.33). Despite the significant changes in P_{wall} values, in practice it is only the variation in the difference that matters in TG-51 because k_Q involves only the ratio of P_{wall} values. This reduces the overall error in TG-51 to less than 0.6% from this effect and for chambers with walls of C552 (air-equivalent plastic) and polymethylmethacrylate (PMMA), the error is less than roughly 0.1%.

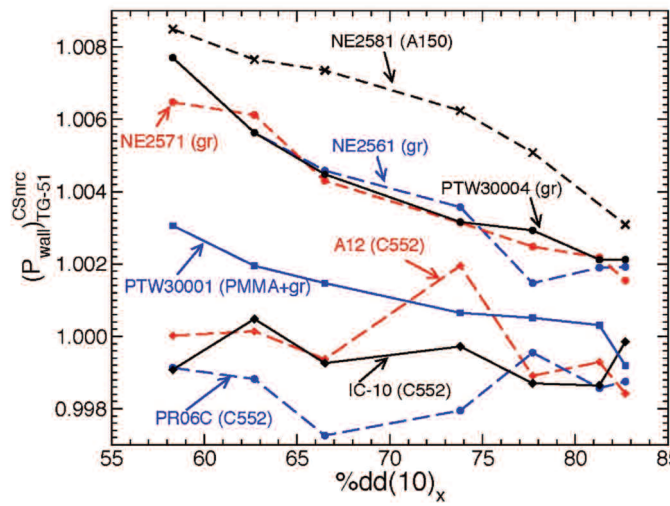

Figure 9-18. Ratio as a function of beam quality %dd(10)$_x$, of the Monte Carlo–calculated, i.e., correct, values of P_{wall} under reference conditions to those calculated by equation (9.33) and used in TG-51. Only the variation of the ratio with beam quality has an effect on TG-51 since it only depends on ratios of P_{wall} values. [Redrawn from Buckley and Rogers (2006b) with permission from American Association of Physicists in Medicine.]

In a more recent study, Wulff et al. (2008b) calculated P_{wall} for an NE2571 as a function of beam quality and got good agreement with the previous Monte Carlo results at the reference depth but also showed that: P_{wall} values increased by about 0.5% as a function of depth in a 10×10 cm^2 field; P_{wall} values on the central axis increase by about 0.6% as the field goes from 10×10 cm^2 to 40×40 cm^2; P_{wall} values decrease by about 0.5% from the central axis to the edge of the field in a 40×40 cm^2 field and then increase by 1.5% passing through the penumbra. While these results do not affect dosimetry under reference conditions, they indicate the difficulty of making clinical ion chamber measurements with accuracy at the 1% level or better.

***P_{wall}* Values for Cylindrical Chambers in Electron Beams.** Although P_{wall} for cylindrical chambers is assumed to be 1.00 in all current dosimetry protocols, Buckley and Rogers (2006b) calculated values at d_{ref} for a variety of common thimble chambers (see figure 9-19). While there is some scatter about the lines shown (±0.1%), the figure shows that there are variations of up to 0.8%, consistent with Nahum's 1988 estimate discussed above. For example, for a beam with R_{50} = 3 cm, one would expect to see a difference of over 0.7% in the doses determined with TG-51 using an NE2581 versus using an A12 chamber because of the use of the wrong values of P_{wall} in the electron beam.

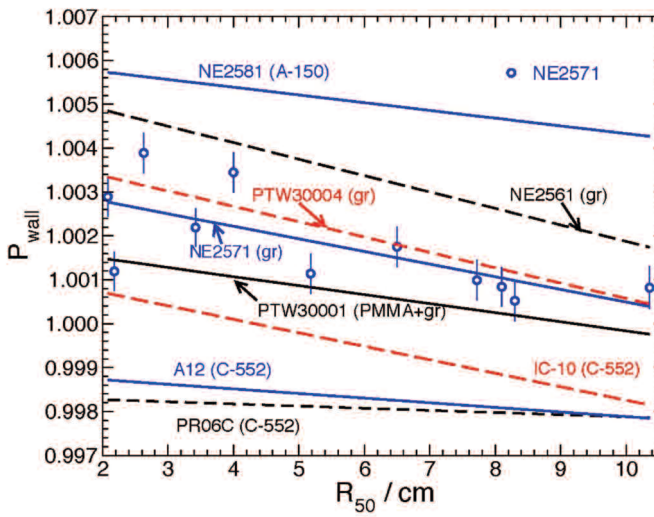

Figure 9-19. Monte Carlo–calculated values of P_{wall} in a water phantom for thimble chambers at d_{ref} in electron beams, as a function of beam quality, R_{50}. Lines represent least squares fits to the raw data, which are scattered. The individual values are shown for the NE2571. [Redrawn from Buckley and Rogers (2006b) with permission from American Association of Physicists in Medicine.]

That same paper showed a dramatic variation in P_{wall} with depth (up to 2.5% increase from the surface to a depth of R_{50} for an NE2571 chamber in a 6 MeV beam). If the density of the graphite wall was reduced to 1.00 g/cm3 in the calculations, the values of P_{wall} decrease by 0.5% with depth rather than increasing. However, the effect cannot be taken into account by a simple depth shift since if that were the case, the P_{wall} correction would be constant in the linear fall-off region of the depth-dose curve, and it continues to increase.

P_{wall} Values for Plane-Parallel Chambers in Electron Beams. In another paper Buckley and Rogers (2006a) reported extensive calculations of P_{wall} corrections for plane-parallel chambers in electron beams. Figure 9-20 shows these values at d_{ref} for four plane-parallel chambers. As discussed above, these results are not particularly surprising but are at odds with the standard assumption of $P_{wall} = 1.0$ made in TG-51 and other protocols. Perhaps most critical is that the largest deviation from unity is for the NACP chamber, which has been used in many measurements of various factors for other chambers under the assumption of a unity value. Zink and Wulff (2008) and Verhaegen et al. (2006) reported calculated P_{wall} values for the Roos and NACP chambers respectively which agreed well with those presented in the figure.

Buckley and Rogers (2006a) and Verhaegen et al. (2006) both calculated values of P_{wall} for the NACP chamber as a function of depth and found values over 1.06 at

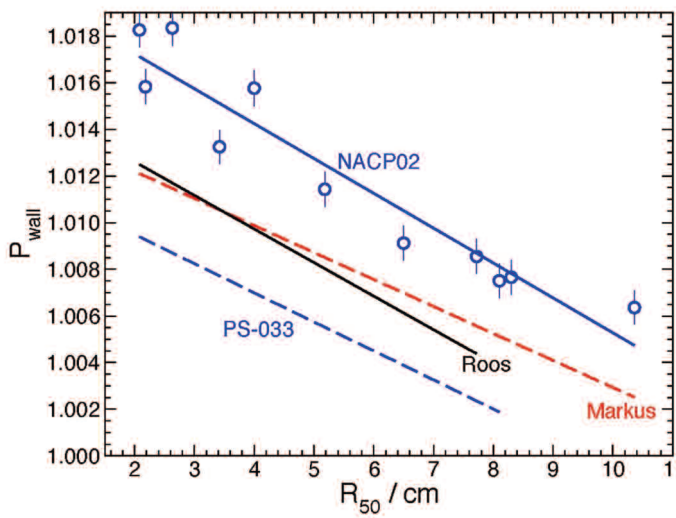

Figure 9-20. Monte Carlo–calculated values of P_{wall} in a water phantom for plane-parallel chambers at d_{ref} in electron beams, as a function of beam quality, R_{50}. Lines represent least squares fits to the raw data, which are quite scattered. The individual values are shown for the NACP02 chamber. [Redrawn from Buckley and Rogers (2006a) with permission from American Association of Physicists in Medicine.]

a depth of R_{50} for a 6 MeV beam and smaller, but nonetheless substantial increases with depth for higher energy beams. As pointed out for the cylindrical chambers, this is at least partially explained by the extra density of the front wall, which is quite thick for the NACP chamber, but it cannot explain it completely since the value does not become constant in the relatively linear fall-off region of the depth-dose curve.

5.4 The Fluence Correction Factor, P_{fl}

The fluence correction factor is discussed in general in section 2.4.6 above. It was pointed out that for photon beams, because the reference depth is in a region of transient charged particle equilibrium, P_{fl} is taken as unity. The details of how P_{fl} is included in TG-51 for electron beams are presented below.

5.4.1 P_{fl} in Electron Beams

Cylindrical Chambers. TG-51 uses the tabulated values of P_{fl} versus $\overline{E}_z$, the mean energy of the electrons at depth z, presented in Table VIII of TG-21. These data are based on measurements by Johansson et al. (1977) at the peak of the depth-ionization curve in a PMMA phantom. In figure 9-21 these data are compared to the

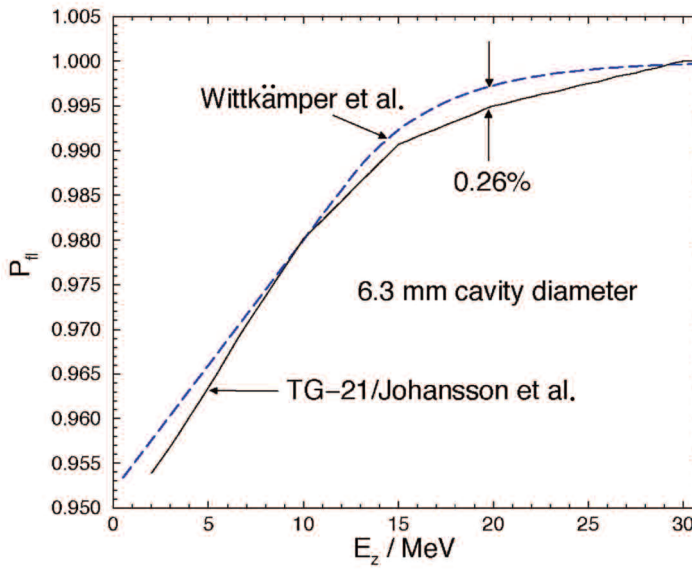

Figure 9-21. Comparison of the values of P_{fl} as a function of $\overline{E}_z$ used in TG-51 (solid) for a chamber with a cavity diameter of 6.3 mm to the fit to their data proposed by Wittkämper et al. (1991) (dashed). The TG-51 data are interpolated from the data in TG-21, which are based on the work of Johansson et al. (1977). The highest energy studied by Wittkämper et al. was 14.2 MeV so the discrepancies at higher energies may not be meaningful.

data of Wittkämper et al. (1991), which were also independently confirmed by Van der Plaetsen et al. (1994). The newer data are for a single chamber (an NE2571 Farmer chamber) so they have not been used in TG-51. However, they suggest that the TG-51 data are accurate at the 0.26% level.

All of the accurately measured values of P_{fl} are at $d_{\max}$ (Johansson et al. 1977; Wittkämper et al. 1991; Van der Plaetsen et al. 1994) and in principle do not apply at depths away from $d_{\max}$, e.g., at d_{ref} for higher-energy electron beams. Nonetheless, TG-51 uses these values at d_{ref} by taking the value of $\overline{E}_z$ at d_{ref} and using the corresponding P_{fl} ($\overline{E}_z$) value determined at $d_{\max}$. There are some measurements which confirm the applicability of these correction factors away from $d_{\max}$ (Huq et al. 1997; Ding and Cygler 1998; Reft and Kuchnir 1999) although the overall uncertainty on measurements such as these is often quite large (i.e., ≥1%).

To determine P_{fl} at the reference depth, TG-51 needed to determine the mean energy at d_{ref}. This was done by using the standard Harder relationship for the mean electron energy at depth z, $\overline{E}_z$ (ICRU 1984a), *viz.*:

$$\overline{E}_z = \overline{E}_o \left(1 - z / R_p\right), \tag{9.35}$$

where $\overline{E}_o$ is the mean electron energy at the surface of the phantom, and R_p is the practical range. Two approximations were used to recast this equation in terms of R_{50}, the beam quality specifier in TG-51. Firstly $\overline{E}_o = 2.33\ R_{50}$, the approximate relationship from TG-21 was used. To establish a relationship between R_p and R_{50}, 21 pairs of these data were taken from the work of Ding and Rogers (1995) (see figure 9-22) and fit to give (Rogers 1996):

$$R_p = 1.2709\ R_{50} - 0.23, \tag{9.36}$$

where R_p and R_{50} are in cm. Hence the mean energy at depth z is given in terms of the beam quality specifier R_{50} as:

$$\overline{E}_o = 2.33\ R_{50}(1 - z/(1.2709\ R_{50} - 0.23)) \quad \text{[MeV]}. \tag{9.37}$$

This Harder relationship is used to assign the mean energy at depth despite the fact that it is approximate (Ding et al. 1996). It is adequate for these purposes and ensures a consistent use of the P_{fl} data, which were originally characterized in the same way. TRS-277 chose to assign $\overline{E}_z$ based on Monte Carlo calculations by Andreo and Brahme (1981) but in principle this leads to an inappropriate selection of P_{fl} unless the mean energies in the Johansson et al. (1977) data are reanalyzed. Also, Ding et al. (1996)'s calculations of mean energy as a function of depth for realistic beams show considerable discrepancy with the earlier calculations for monoenergetic beams (Andreo and Brahme 1981).

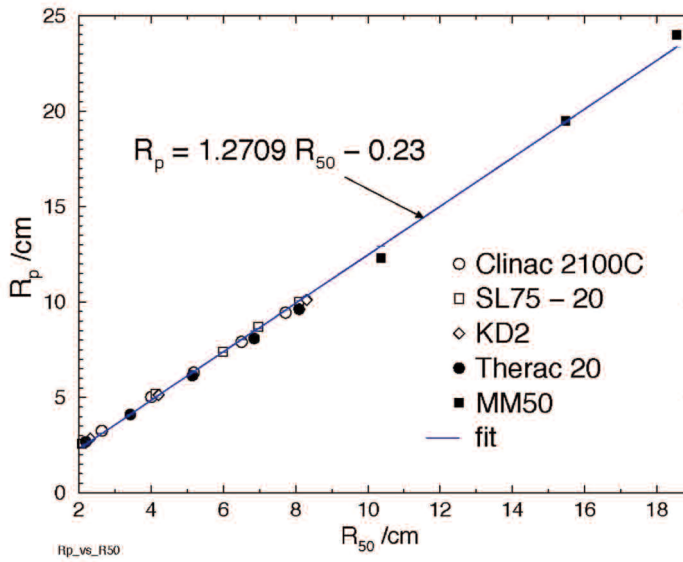

Figure 9-22. Linear relationship between R_{50}, the depth at which the dose falls to 50% of dose maximum, and the R_p, the practical range, based on fitting 21 pairs of calculated data points from Ding and Rogers (1995).

Plane-Parallel Chambers. The fluence correction for well-guarded plane-parallel chambers is taken as unity (Almond et al. 1994). However, many authors have shown that the Markus and Capintec plane-parallel chambers have substantial fluence corrections (see TG-39 and references therein, Almond et al. 1994), especially at low energies. Unfortunately, these are very difficult measurements to make and the scatter in experimental results is substantial. Nonetheless TG-39 recommended values for P_{fl} as a function of mean electron energy at depth. These values are used in TG-51 and presented in figure 9-23. The method for determining $\overline{E}_z$ described in the previous section is also used with plane-parallel chambers.

5.5 The Gradient Correction Factor, P_{gr}

As discussed in section 2.4.6, for electron beams the gradient correction is based on a simple measurement in the user's beam and application of equation (9.18). This is equivalent to using an effective point of measurement as done in TRS-398.

For photon beams, gradient correction factors in various protocols are based on different sources. TG-21 based its values on the work of Cunningham and Sontag (1980), which is a mixture of experiment and mostly calculations. TRS-398 uses

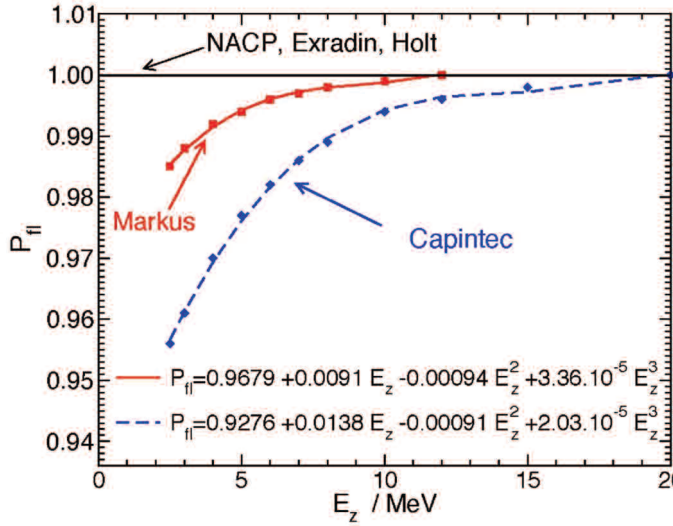

Figure 9-23. The P_{fl} factors for plane-parallel chambers recommended by TG-39 (Almond et al. 1994) and used in TG-51. Also shown are cubic fits to the curves used by TG-51 for the Markus and Capintec chambers. The factors are given as a function of $\bar{E}_z$, the mean energy at the depth of measurement. These fits were not actually needed since TG-39 presented a similar characterization, but this is what was used in TG-51.

the measured data of Johansson et al. (1977) for the displacement factor, *DF,* to estimate the gradient correction as:

$$P_{gr}^{398} = 1 - D\,F\,r_{\text{cav}}, \tag{9.38}$$

where Andreo has done a fit to interpolate the Johansson et al. data as a function of TPR_{10}^{20} (Andreo, private communication, 2008). One can also estimate the effective P_{gr} value caused by using a given offset of the effective point of measurement as (Rogers and Ross 1992):

$$P_{gr}^{offset} = 1 + \left(\frac{1}{10}\ln\frac{D_{20}}{D_{10}}\right)\Delta z, \tag{9.39}$$

where Δz is the chamber offset (0.6 r_{cav} or 0.75 r_{cav}) and the ratio of doses at 20 and 10 cm is determined from the value of TPR_{10}^{20} using a linear fit (Rogers and Booth 2009) to the data in Table XIII of TRS-277, *viz.*:

$$\frac{D_{20}}{D_{10}} = 0.05607 + 0.77639\ \text{TPR}_{10}^{20}. \tag{9.40}$$

This fit is in excellent agreement with the relationship published by Followill et al. (1998) based on extensive Radiological Physics Center (RPC) measurements.

Since $\ln(D_{20}/D_{10})$ is negative, equation (9.39) implies P_{gr}^{offset} is less than 1 which physically corresponds to the fact that when an ion chamber is centered at depth z, the effective point of measurement is upstream where the dose is higher and must therefore be reduced by P_{gr} to get the correct reading at depth z.

Figure 9-24 presents a comparison of the various values of P_{gr}. The difference between the AAPM values and the TRS-398 values is up to 0.5%. The TRS-398 values fluctuate slightly about the effective P_{gr} value for an offset of 0.6 r_{cav}, consistent with the fact that both sets of values are based on different sets of data from Johansson et al. (1977).

TG-51 uses the Cunningham and Sontag (1980) data for P_{gr} as used in TG-21 and shown in figure 9-24. This is done by interpolating a digitized version of Figure 5 of the TG-21 protocol and converting the $\%dd(10)_x$ beam quality specifier to NAP in the same way as described in section 5.3.1 via equation (9.30).

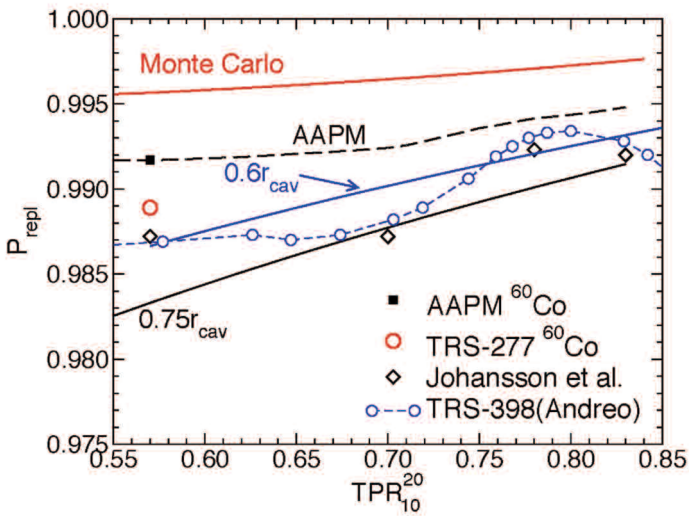

Figure 9-24. Value of P_{repl} (= P_{gr} in a photon beam), for a 6.4 mm cavity, as a function of beam quality specified by TPR_{10}^{20}. The AAPM values were used in TG-51 and TG-21, based on the work of Cunningham and Sontag (1980). The two lower solid lines are the effective values based on equaton (9.39) corresponding to offsets of 0.75 r_{cav} (as used in TRS-277), 0.6 r_{cav} (as used in TRS-398 and TG-51 for depth-dose curve measurements). The values based on the displacement factor measurements of Johansson et al. (1977) are shown as diamonds and the values used in TRS-398 to calculate k_Q are shown as a broken line with symbols (from Andreo's fit to the data of Johansson et al. 1977). The recent Monte Carlo–calculated values are shown as the upper solid line. [Reprinted from Wang and Rogers (2009b) with permission from American Association of Physicists in Medicine.]

5.5.1 P_{repl}: State-of-the-Art

The values of the P_{repl} correction used by TG-51 and TRS-398 for photon beams are the largest differences between these protocols because they are based on different data sources. However, in the end, the ratio of the P_{repl} values is what is used in the protocols and these do not differ as much because the curves in figure 9-24 are nearly parallel. Until recently this was also a very difficult correction to calculate with Monte Carlo techniques because, unlike many other correction factors, it requires the correct absolute calculation of the dose in a cavity rather than just a ratio of two related quantities as needed for P_{wall} or K_{wall}. Wang and Rogers (2008b) showed that EGS4 calculations of this quantity were wrong by roughly 1% because of EGS4's known systematic uncertainty calculating ion chamber response. In addition, the calculations are extremely time consuming since they require calculations of the dose to the cavity in a phantom at the reference depth.

Wang and Rogers (2008a) evaluated four methods to calculate P_{repl} using Monte Carlo techniques. Two were direct methods, independent of the calculation of the water to air stopping-power ratio, which thereby avoids uncertainties regarding the appropriate selection of Δ. For the case of photon beams and plane-parallel chambers in electron beams it was shown that the four proposed methods gave the same answers within about 0.1%, which was reassuring since most previous calculations had depended on one of the indirect methods. However, Wang and Rogers (2009a) showed that not all these techniques worked for cylindrical chambers in electron beams because there is no longer transient charged particle equilibrium.

P_{repl} or P_{gr} Corrections for Cylindrical Chambers in Photon Beams. With the new ability to calculate P_{repl} (i.e., P_{gr} because P_{fl} is unity past $d_{\max}$) directly for photon beams, Wang and Rogers (2008a) found that the correct value was considerably closer to unity than the previous values. For example the value for a Farmer-like chamber in a ^{60}Co beam was 0.9964 compared to the values of 0.992 and 0.988 used in TG-51 and TRS-398, respectively. Wulff et al. (2008a) calculated similar values for an NE2571 chamber. Wang and Rogers (2008a) demonstrated that their calculations could match the measured values in Cunningham and Sontag (1980) which were used to extract the P_{repl} values used in TG-21 and TG-51, but that the explicit calculation of the P_{repl} value was different, i.e., the interpretation of the earlier results in terms of P_{repl} was incorrect. Similarly, Wang and Rogers (2009c) demonstrated that the interpretation of the measurements in Johansson et al. (1977) is incorrect, and that a proper interpretation leads to values consistent with the new calculations of P_{repl}. These new values are shown in figure 9-24 and are seen to be considerably closer to unity than the previous values. Figure 9-25 shows the ratios of P_{repl} values as a function of beam quality since it is only the ratios which appear in the TG-51 protocol and it can be seen that there is little change in the ratios despite the overall change in P_{repl} values.

In addition to finding new values for P_{repl} in photon beams, Wang and Rogers (2008a) studied the value as a function of cavity length and found that is was only

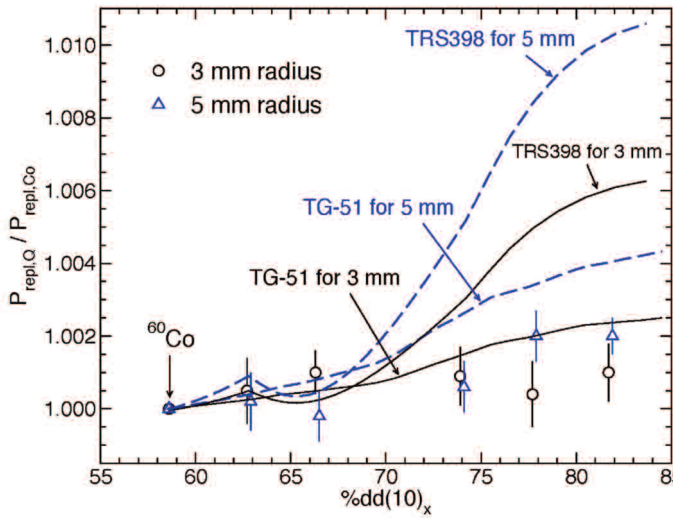

Figure 9-25. The beam quality dependence of the ratio of P_{repl} values for a beam of quality Q to that of ^{60}Co for both a Farmer-type chamber (3 mm radius) and a larger cylindrical chamber (5 mm radius). The symbols are calculated in this study and the lines are the values used in either TG-51 (TG-21) or IAEA's TRS-398. [Reprinted from *Physics in Medicine and Biology,* "The replacement correction factors for cylindrical chambers in high-energy photon beams." L. L. W. Wang and D. W. O. Rogers, vol 54, pp. 1609–1620. © 2009 with permission from IOP Publishing.)

weakly dependent on the length from 5 to 20 mm (0.2% increase), which is consistent with the assumed lack of any dependence in all protocols.

***P_{repl}* Corrections for Cylindrical Chambers in Electron Beams.** Wang and Rogers (2009a) have shown that the issue of P_{repl} for cylindrical chambers in electron beams is complex because the spectrum of electrons at the effective point of measurement is quite different from that in the phantom at the point corresponding to the center of the ion chamber. The same paper shows that selecting the offset for the effective point of measurement can be done in two ways. One is to minimize the difference between the depth-ionization and depth-dose curves after correcting for the stopping-power ratio, in which case one finds that an offset of about 0.5 r_{cav} is correct. Another method is to match the spectrum in the ion chamber to the spectrum at the effective point of measurement in the phantom, in which case an offset of about 0.8 r_{cav} is appropriate. Figure 9-26a shows that when parameterized in terms of the mean energy at the point of measurement, P_{fl} values at d_{ref} and at $d_{\max}$ are on a single curve, thereby justifying this approach in TG-51. Figure 9-26b shows that the Monte Carlo calculated P_{fl} values at d_{ref} are in reasonably good

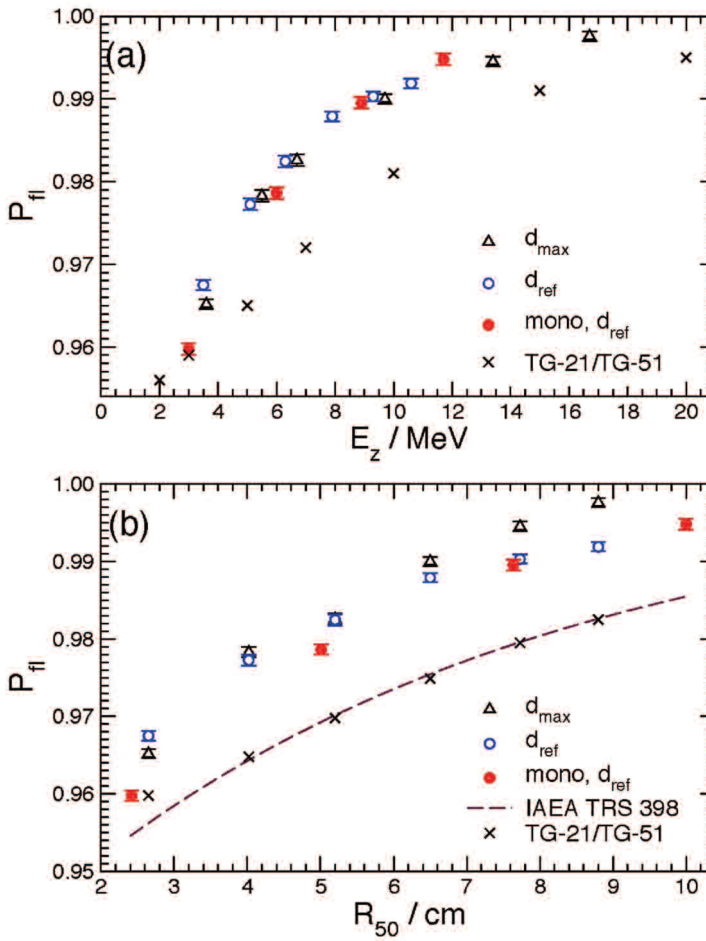

Figure 9-26. (a) The calculated P_{fl} values for a Farmer chamber in electron beams as a function of the mean electron energy at depth. P_{fl} values at d_{max} and/or at d_{ref} for both real linac beams (open symbols) and monoenergetic beams (solid symbols) are shown. The cross symbols are the TG-21 values (used in TG-51) based on Johansson et al.'s measurement (1977) at d_{max}. (b) Same data sets as in (a) but with R_{50} as the beam quality specifier. The dashed line and x's are the P_{fl} (p_{cav}) values used in TRS-398 and TG-51, respectively. [Reprinted from Wang and Rogers (2009b) with permission from American Association of Physicists in Medicine.]

agreement with those currently in use based on the measurements of Johansson et al. (1977), although the new values do tend to be 0.5% to 1.0% closer to unity, which reflects the incorrect assumption in the original measurements that P_{wall} is unity for a plane-parallel chamber in a high-energy electron beam.

P_{repl} Corrections for Plane-Parallel Chambers in Electron Beams. Although P_{repl} is considered unity for well-guarded plane-parallel chambers, various Monte Carlo studies have indicated considerable variation with depth (Buckley and Rogers 2006a; Verhaegen et al. 2006; Wang and Rogers 2008a). The values for the NACP chamber at d_{ref} vary between 0.996 in a 6 MeV beam to 1.0005 in an 18 MeV beam (Wang and Rogers 2008a) and for the Roos chamber the values fluctuate between 0.997 and 1.003 (Zink and Wulff 2008). The major impact of these apparently non-unity values is that they imply many measured values for both cylindrical and plane-parallel chambers contain systematic errors because of the assumed value of unity.

The more significant issue in clinical practice is the value of P_{repl} at depth where the NACP chamber's P_{repl} value is greater than 1.03 at R_{50} (Wang and Rogers 2008a).

6. The P_{ion} Equation

The correction for ion recombination has been extensively studied and Boag (1987) gives a general introduction to the details of the physics and chapter 6 outlines it.

TG-51 uses two-voltage techniques for determining the P_{ion} correction. Let V_H be the normal operating voltage for the detector (always the higher of the two voltages in these measurements) and M_{raw}^{H} be the raw chamber reading with bias V_H. After measuring M_{raw}^{H} the detector bias is reduced by at least a factor of 2 to V_L and M_{raw}^{L} is measured once the chamber readings have reached equilibrium.

For continuous ^{60}Co beams, the underlying theory for general recombination gives:

$$P_{ion} = \frac{M_{sat}}{M} = 1 + \frac{C M_{sat}}{V^2}, \tag{9.41}$$

where C is a constant. From this one can derive the two-voltage formula by algebraic manipulation or by considering a plot of $\frac{1}{M}$ vs. $\frac{1}{V^2}$ (Almond 1981; Weinhous and Meli 1984):

$$P_{ion}\left(V_H\right) = \frac{1. - \left(\frac{V_H}{V_L}\right)^2}{\frac{M_{raw}^{H}}{M_{raw}^{L}} - \left(\frac{V_H}{V_L}\right)^2}. \tag{9.42}$$

Equation (9.42) provides an estimate of the general recombination in the continuous beam. This is what TG-51 uses although though initial recombination may dominate, in which case equation (9.46) may be more appropriate.

The exact equations for pulsed or pulsed-swept beams are nonlinear (Weinhous and Meli 1984). From the underlying theory, for a pulsed beam one has:

$$P_{ion} = \frac{M_{sat}}{M} = \frac{u}{\ln(1+u)}, \tag{9.43}$$

where $u = C''/V$ with C'' a constant. From this relationship one can show that:

$$\frac{M_H}{M_L} = \frac{V_H}{V_L} \frac{\ln(1+u_H)}{\ln\left(1+u_H \frac{V_H}{V_L}\right)}. \tag{9.44}$$

Weinhous and Meli (1984) solved this equation numerically for u_H given V_H/V_L and M_H/M_L. Then, P_{ion} can be calculated using equation (9.43).

However, for small values of u_H, $\ln(1 + u_H)$ can be approximated as $u_H - \frac{1}{2}u_H^2$ so that:

$$P_{ion} = 1 + \frac{C'}{V}, \tag{9.45}$$

and hence for pulsed beams with $P_{ion} < 1.05$ one can show, using a plot of $\frac{1}{M}$ vs. $\frac{1}{V}$, that:

$$P_{ion}(V_H) = \frac{1. - \frac{V_H}{V_L}}{\frac{M^H_{raw}}{M^L_{raw}} - \frac{V_H}{V_L}}. \tag{9.46}$$

Although pulsed swept beams no longer appear to be used, the same equation applies to that case despite having a different form of exact equation.

Equation (9.46) gives the same result as solving the exact nonlinear equations for pulsed or pulsed swept beams to within 0.2% and 0.4%, respectively, for a voltage ratio of 2 and 0.3% and 0.6% for a voltage ratio of 3 and is most inaccurate at the limiting value of P_{ion} = 1.05; i.e., it is much more accurate for values of P_{ion} closer to unity. Figure 9-27 presents a comparison of the results for the equation used in TG-51 for pulsed and pulsed swept beams compared to the "exact" solution of Boag's equations using the algorithm of Weinhous and Meli (1984).

For larger values of the voltage ratio or values of P_{ion} near 1.05 one may use the published programs or fits for the nonlinear equations (Weinhous and Meli 1984; Schulz et al. 1986).

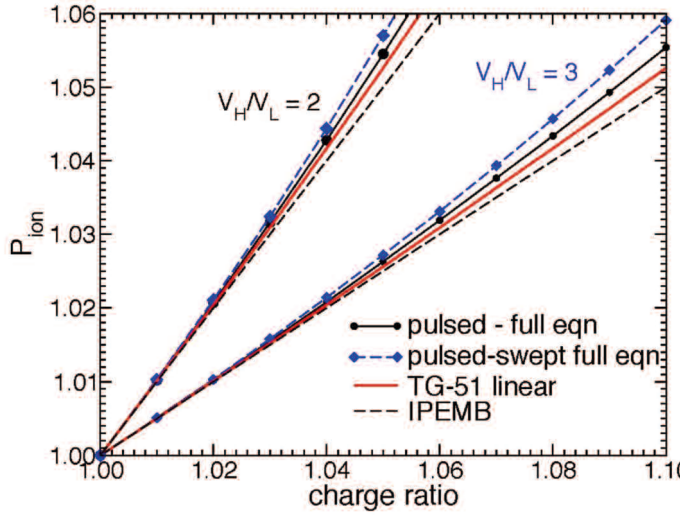

Figure 9-27. Comparison of the value of P_{ion} predicted by the equation for pulsed and pulsed swept beams given in TG-51 (solid) compared to the exact solutions as given by the algorithm of Weinhous and Meli (1984) and the equation in the IPEMB protocol (Thwaites et al. 1996). Voltage ratio is either 2 or 3.

The British Code of Practice (Thwaites et al. 1996) also presents a linearized form of these equations, *viz.*:

$$P_{ion}\left(V_H\right) = 1 + \frac{\left(\frac{M^H_{raw}}{M^L_{raw}} - 1\right)}{\left(\frac{V_H}{V_L} - 1\right)}, \tag{9.47}$$

but it is clear from figure 9-27 that equation (9.46) is slightly more accurate.

7. Electron Beam Depth-Dose Curves

TG-51 (and TRS-398) determine the absorbed dose to water at the reference depth based on the stopping-power ratios calculated by Ding et al. (1995) for realistic electron beams. For consistency these data must be used to derive the stopping-power ratio at other depths when converting a measured depth-ionization distribution to a

depth-dose distribution. Burns et al. (1996) gave an expression for the stopping-power ratio as a function of R_{50} and depth based on a fit to the $\left(\bar{L}/\rho\right)_{air}^{water}$ versus depth data for 24 realistic electron beams (Ding et al. 1995; Ding and Rogers 1993). The R_{50} values that were fit range from 0.98 cm to 18.6 cm and values for z/R_{50} range from 0.02 to 1.2.

The best least squares universal fit to the data is:

$$\left(\frac{\bar{L}}{\rho}\right)_{air}^{water}\left(R_{50},z\right)=\frac{a+b\left(\ln R_{50}\right)+c\left(\ln R_{50}\right)^2+d\left(z/\ln R_{50}\right)}{1+e\left(\ln R_{50}\right)+f\left(\ln R_{50}\right)^2+g\left(\ln R_{50}\right)^3+h\left(z/\ln R_{50}\right)}. \qquad (9.48)$$

a = 1.0752 b = –0.50867 c = 0.088670 d = –0.08402
e = –0.42806 f = 0.064627 g = 0.003085 h = –0.12460

The values for the eight coefficients given above result in an rms deviation of 0.4% and a maximum deviation of 1.0% for z/ R_{50} ranging between 0.02 and 1.1 for the full range of beam qualities (1 cm < R_{50} < 18.6 cm). The maximum deviation increases to 1.7% for z/ R_{50} values up to 1.2 and is much worse at deeper depths (see Rogers 2004).

The universal fit is best applied to relative calculations and in particular to the conversion of a measured depth-ionization distribution into a depth-dose distribution (which, in principle, also requires taking into account any changes in other factors such as P_{wall} and P_{repl}). For the determination of the stopping-power ratio at the reference depth, equation (9.28) should be used.

8. Experimental Verification of k_Q Values for Photon Beams

There have been a wide variety of measurements of k_Q values. Some of these are summarized in figure 9-28 for the NE2571 chamber. Given the measurement uncertainties, it is clear that the TG-51 calculated values of k_Q are in good agreement with the measured values. Seuntjens et al. (2000) was the most extensive, highest precision study which included measurements for 20 different ion chambers of six different makes. The rms deviation between the measured k_Q values and the TG-51 calculated values was 0.41% with an uncertainty on the individual measurements of 0.36%. This suggests that the uncertainty on the calculated values of k_Q is of the order of 0.4%.

9. Summary

The physics of the TG-51 protocol was firmly built on the physics in the TG-21 protocol. A great simplification was possible in TG-51 due to using calibrations based on absorbed-dose primary standards. Unlike TG-21 where a large number of logical and physical data inconsistencies were discovered over the years after publi-

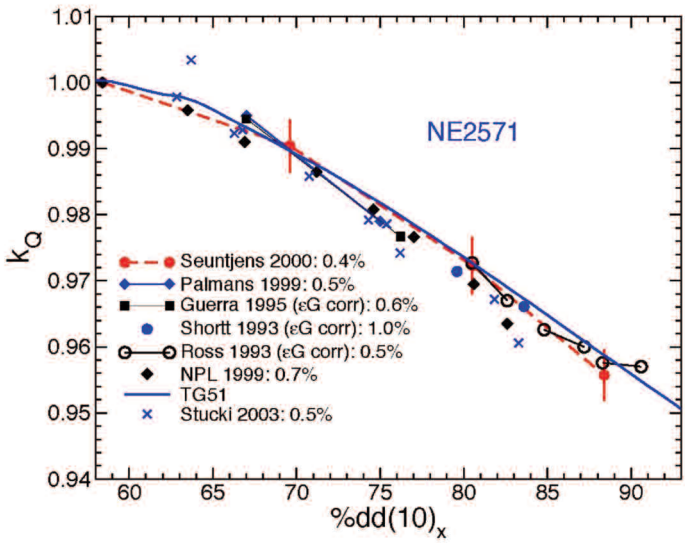

Figure 9-28. Comparison of measured values of k_Q to those given in TG-51 for the NE2571 ion chamber. Most data are taken from Seuntjens et al. (2000). The Seuntjens, Stucki, and Palmans data are based on sealed water calorimeters, the NPL data on a graphite calorimeter, and the other measurements on Fricke dosimetry where the original results have been systematically corrected for the variation in εG reported by Klassen et al. (1999). Stated uncertainties are given in the legend. Full references to original sources are included in Seuntjens et al. (2000) and Aalbers et al. (2008).

cation, so far there have been no major errata required for TG-51, although, as indicated throughout this chapter, there have been a variety of advances in our understanding which could impact various aspects of the protocol. Nonetheless, the experimental verification of the calculated k_Q factors for photon beams suggest that whatever improvements there may be, the overall changes required remain small. There is still room for more study in electron beams where the potential changes seem more important. The development of primary standards of absorbed dose that can be used reliably in electron beams will be of direct interest.

Acknowledgments

I want to thank my colleagues on Task Group 51, Peter Almond, Peter Biggs, Bert Coursey, Will Hanson, Saiful Huq, and Ravi Nath for many thought-provoking and enjoyable discussions over the years that the protocol was being developed. I also thank two of my doctoral students at Carleton University, Lesley Buckley and Lilie Wang, who devoted several years of their lives to developing the tools and expertise to nail down P_{wall} and P_{repl} correction factors. I thank Pedro Andreo for permission to

quote his calculated values of P_{gr} used in TRS-398. This work was supported by NSERC, the Canada Research Chairs program and the National Research Council of Canada where much of the original work was done.

References

Aalbers, A. H. L., M. T. Hoornaert, A. Minken, H. Palmans, M. W. H. Pieksma, L. A. de Prez, N. Reynaert, S. Vynckier, and F. W. Wittkämper. (2008). Code of Practice for the Absorbed Dose Determination in High Energy Photon and Electron Beams. NCS Report 18 of The Netherlands Commission on Radiation Dosimetry.

AAPM TG–21 (1983). "A protocol for the determination of absorbed dose from high-energy photon and electron beams." *Med Phys* 10:741–771.

Almond, P. R. (1981). "Use of a Victoreen 500 electrometer to determine ionization chamber collection efficiencies." *Med Phys* 8:901–904.

Almond, P. R., and H. Svensson. (1977). "Ionization chamber dosimetry for photon and electron beams." *Acta Radiol Ther Phys Biol* 16:177–186.

Almond, P. R., F. H. Attix, S. Goetsch, L. J. Humphries, H. Kubo, R. Nath, and D. W. O. Rogers. (1994). "The calibration and use of plane-parallel ionization chambers for dosimetry of electron beams: An extension of the 1983 AAPM protocol report of AAPM Radiation Therapy Committee Task Group 39." *Med Phys* 21:1251–1260. Also available as AAPM Report No. 48.

Almond, P. R., P. J. Biggs, B. M. Coursey, W. F. Hanson, M. S. Huq, R. Nath, and D. W. O. Rogers. (1999). "AAPM's TG–51 protocol for clinical reference dosimetry of high-energy photon and electron beams." *Med Phys* 26:1847–1870. Also available as AAPM Report No. 67.

Andreo, P. (2000). "A comparison between calculated and experimental k_Q photon beam quality correction factors." *Phys Med Biol* 45:L25–L38.

Andreo. P. (1992). "Absorbed dose beam quality factors for the dosimetry of high-energy photon beams." *Phys Med Biol* 37:2189–2211.

Andreo, P., and A. Brahme. (1981). "Mean energy in electron beams." *Med Phys* 8:682–687.

Araki, F., R. Ikeda, Y. Shirakawa, T. Shimonobou, N. Moribe, T. Takada, M. Takahashi, H. Oura, and M. Matoba. (2000). "Wall correction factors for calibration of plane-parallel ionization chambers with high-energy photon beams." *Phys Med Biol* 45:2509–2517.

Attix, F. H. *Introduction to Radiological Physics and Radiation Dosimetry.* New York: John Wiley & Sons, 1986.

Berger, M. J., and S. M. Seltzer. (1983). Stopping Power and Ranges of Electrons and Positrons. NBS Report NBSIR 82-2550-A (Second edition). Gaithersburg, MD: NBS.

Bichsel, H., and T. Hiraoka. (1992). "Energy loss of 70 MeV protons in elements." *Nucl Instrum Meth B* 66:345–351.

Boag, J. W. "Ionization Chambers" in *The Dosimetry of Ionizing Radiation,* Vol II. K. R. Kase, B. E. Bjärngard, and F. H. Attix (eds.). San Diego, CA: Academic Press, pp. 169–243, 1987.

Boutillon, M., and A. M. Perroche-Roux. (1987). "Re-evaluation of the W value for electrons in dry air." *Phys Med Biol* 32:213–219.

Buckley, L. A., and D. W. O. Rogers. (2006a). "Wall correction factors, P_{wall}, for parallel-plate ionization chambers." *Med Phys* 33:1788–1796.

Buckley, L. A., and D. W. O. Rogers. (2006b). "Wall correction factors, P_{wall}, for thimble ionization chambers." *Med Phys* 33:455–464.

Buckley, L. A., I. Kawrakow, and D. W. O. Rogers. (2004). "CSnrc: Correlated sampling Monte Carlo calculations using EGSnrc." *Med Phys* 31:3425–3435.

Buckley, L. A., I. Kawrakow, and D. W. O. Rogers. (2003). "An EGSnrc investigation of cavity theory for ion chambers measuring air kerma." *Med Phys* 30:1211–1218.

Burns, D. T., G. X. Ding, and D. W. O. Rogers. (1996). "R_{50} as a beam quality specifier for selecting stopping-power ratios and reference depths for electron dosimetry." Med Phys 23:383–388.

Christ, G., O. S. Dohm, G. Bruggmoser, and E. Schüle. (2002). "The use of plane-parallel chambers in electron dosimetry without any cross-calibration." *Phys Med Biol* 47:N121–N126.

Cunningham, J. R., and R. J. Schulz. (1984). "On the selection of stopping-power and mass-energy absorption coefficient ratios for high energy x-ray dosimetry." *Med Phys* 11: 618–623.

Cunningham, J. R., and M. R. Sontag. (1980). "Displacement corrections used in absorbed dose determinations." *Med Phys* 7:672–676.

Cunningham, J. R., M. Woo, D. W. O. Rogers, and A. F. Bielajew. (1986). "The dependence of mass energy absorption coefficient ratios on beam size and depth in a phantom." *Med Phys* 13:496–502.

Ding, G. X., and J. Cygler. (1998). "Measurement of P_{repl} P_{wall} factors in electron beams and in a ^{60}Co beam for plane-parallel chambers." *Med Phys* 25:1453–1457.

Ding, G. X., and D. W. O. Rogers. (1995). Energy Spectra, Angular Spread, and Dose Distributions of Electron Beams from Various Accelerators Used in Radiotherapy. NRC Report PIRS–0439. Ottawa: National Research Council.

Ding, G. X., and D. W. O. Rogers. (1993). Monte Carlo Simulation of NPL Linac and Calculation of Dose Distributions and Water/Air Stopping-Power Ratios. NRC Report PIRS–0399. Ottawa: National Research Council.

Ding, G. X., D. W. O. Rogers, and T. R. Mackie. (1996). "Mean energy, energy-range relationship and depth-scaling factors for clinical electron beams." *Med Phys* 23:361–376.

Ding, G. X., D. W. O. Rogers, and T. R. Mackie. (1995). "Calculation of stopping-power ratios using realistic clinical electron beams." *Med Phys* 22:489–501.

Dohm, O. S., G. Christ, F. Nüsslin, E. Schüle, and G. Bruggmoser. (2001). "Electron dosimetry based on the absorbed dose to water concept: A comparison of the AAPM TG–51 and DIN 6800-2 protocols." *Med Phys* 28:2258–2264.

Domen, S. R., and P. J. Lamperti. (1976). "Comparisons of calorimetric and ionometric measurements in graphite irradiated with electrons from 15 to 50 MeV." *Med Phys* 3: 294–301.

Followill, D. S., R. C. Tailor, V. M. Tello, and W. F. Hanson. (1998). "An empirical relationship for determining photon beam quality in TG–21 from a ratio of percent depth doses." *Med Phys* 25:1202–1205.

Gillin, M. T., R. W. Kline, A. Niroomand-Rad, and D. F. Grimm. (1985). "The effect of thickness of the waterproofing sheath on the calibration of photon and electron beams." *Med Phys* 12:234– 236.

Hanson, W. F., and J. A. D. Tinoco. (1985). "Effects of plastic protective caps on the calibration of therapy beams in water." *Med Phys* 12:243–248.

Hohlfeld, K. (1988). "The Standard DIN 6800: Procedures for Absorbed Dose Determination in Radiology by the Ionization Method" in Proceedings of 1987 Symposium on Dosimetry in Radiotherapy, Vol 1, pp. 13–24. Vienna, Austria: IAEA.

Hubbell, J. H. (1982). "Photon mass attenuation and energy-absorption coefficients from 1 keV to 20 MeV." *Int J Appl Radiat Isot* 33:1269–1290.

Hunt, M. A., G. J. Kutcher. and A. Buffa. (1988). "Electron backscatter correction for parallel-plate chambers." *Med Phys* 15:96–103.

Huq, M. S., N. Yue, and N. Suntharalingam. (1997). "Experimental determination of fluence correction factors at depths beyond d_{max} for a Farmer type cylindrical ionization chamber in clinical electron beams." *Med Phys* 24:1609–1613.

IAEA (2000). International Atomic Energy Agency. Absorbed Dose Determination in External Beam Radiotherapy: An International Code of Practice for Dosimetry Based on Standards of Absorbed Dose to Water. Technical Report Series (TRS) No. 398. Vienna, Austria: IAEA.

IAEA (1987). International Atomic Energy Agency. Absorbed Dose Determination in Photon and Electron Beams; An International Code of Practice. Technical Report Series (TRS) No. 277. Vienna, Austria: IAEA.

ICRU (1984a). International Commission on Radiation Units and Measurements. Radiation Dosimetry: Electron Beams with Energies Between 1 and 50 MeV. ICRU Report 35, Washington D.C., ICRU.

ICRU (1984b). International Commission on Radiation Units and Measurements. Stopping Powers for Electrons and Positrons, ICRU Report 37. Bethesda, MD: ICRU.

ICRU (1979). International Commission on Radiation Units and Measurements. Average Energy Required to Produce an Ion Pair. ICRU Report 31. Washington D.C.: ICRU.

Johansson, K. A., L. O. Mattsson, L. Lindborg, and H. Svensson. (1977). "Absorbed-Dose Determination with Ionization Chambers in Electron and Photon Beams Having Energies Between 1 and 50 MeV" in IAEA Symposium Proceedings, pp. 243–270. IAEA–SM– 222/35. Vienna, Austria: IAEA.

Johns, H. E., and J. R. Cunningham. *The Physics of Radiology,* 4th ed. Springfield, IL: Charles C Thomas, 1983.

Kalach, N. I., and D. W. O. Rogers. (2003). "Which accelerator photon beams are 'clinic-like' for reference dosimetry purposes?" *Med Phys* 30:1546–1555.

Kapsch, R. P., G. Bruggmoser, G. Christ, O. S. Dohm, G. H. Hartmann, and E. Schüle. (2007). "Experimental determination of pCo perturbation factors for plane-parallel chambers." *Phys Med Biol* 52:7167–7181.

Kawrakow, I. (2000). "Accurate condensed history Monte Carlo simulation of electron transport. II. Application to ion chamber response simulations." *Med Phys* 27:499–513.

Khan, F. M., K. P. Doppke, K. R. Hogstrom, G. J. Kutcher, R. Nath, S. C. Prasad, J. A. Purdy, M. Rozenfeld, and B. L. Werner. (1991). "Clinical electron-beam dosimetry: Report of AAPM Radiation Therapy Committee Task Group 25." *Med Phys* 18:73–109. Also available as AAPM Report No. 32.

Klassen, N. V., K. R. Shortt, J. P. Seuntjens, and C. K. Ross. (1999). "Fricke dosimetry: The difference between $G(Fe^{3+})$ for ^{60}Co γ-rays and high-energy x-rays." *Phys Med Biol* 44: 1609–1624.

Klevenhagen, S. C. (1994). "An algorithm to include the bremsstrahlung contamination in the determination of the absorbed dose in electron beams." *Phys Med Biol* 39:1103–1112.

Klevenhagen, S. C. (1991). "Implications of electron backscatter for electron dosimetry." *Phys Med Biol* 36:1013–1018.

Kosunen, A., H. Järvinen, and P. Sipilä. (1994). Optimum Calibration of NACP type Plane-Parallel Ionization Chambers for Absorbed Dose Determinations in Low Energy Electron Beams" in Proceedings of a Symposium on Measurement Assurance in Dosimetry, pp. 505– 513. IAEA–SM–330/419. Vienna, Austria: IAEA.

Kosunen, A., and D. W. O. Rogers. (1993). "Beam quality specification for photon beam dosimetry." *Med Phys* 20:1181–1188.

Laitano, R. F., A. S. Guerra, M. Pimpinella, H. Nyström, M. Karlsson, and H. Svensson. (1993). "Correction factors for calibration of plane-parallel ionization chambers with a ^{60}Co gamma-ray beam." *Phys Med Biol* 38:39–54.

Li, X. A., and D. W. O. Rogers. (1994). "Reducing electron contamination for photon-beam-quality specification." *Med Phys* 21:791–798.

Ma, C.-M., and A. E. Nahum. (1993). "Effect of size and composition of central electrode on the response of cylindrical ionisation chambers in high-energy photon and electron beams." *Phys Med Biol* 38:267–290.

Ma, C.-M., and D. W. O. Rogers. (1995). "Monte Carlo Calculated Wall Correction Factors for Plane-Parallel Chambers in High-Energy Electron Beams" in Proceedings of the 1995 COMP Annual Meeting (Canadian Organization of Medical Physicists, Edmonton, Alberta), pp. 117–118.

Mainegra-Hing, E., I. Kawrakow, and D. W. O. Rogers. (2003). "Calculations for plane-parallel ion chambers in ^{60}Co beams using the EGSnrc Monte Carlo code." *Med Phys* 30:179–189.

Mijnheer, B. J., and J. R. Williams. (1985). "Comments on dry air or humid air values for physical parameters used in the AAPM protocol for photon and electron dosimetry." *Med Phys* 12:656–658.

Nahum, A. E. (1988). Extension of the Spencer-Attix Cavity Theory to the 3-Media Situation for Electron Beams In Dosimetry in Radiotherapy, Vol 1, pp. 87–115. Vienna: IAEA.

Nahum, A. E. (1994). Perturbation Effects in Dosimetry. Technical Report ICR-PHYS-1/94. Joint Department of Physics, The Royal Marsden Hospital, Sutton, Surrey, UK.

Palm, Å., and O. Mattsson. (1999). "Experimental study on the influence of the central electrode in Farmer-type ionization chambers." *Phys Med Biol* 44:1299–1308.

Palm Å, O. Mattsson, and P. Andreo. (2000). "Calibration of plane-parallel chambers and determination of P_{wall} for the NACP and Roos chambers for ^{60}Co γ-ray beams." *Phys Med Biol* 45:971–981.

Reft, C. S., and F. T. Kuchnir. (1999). "Measured overall perturbation factors at depths greater than $d_{\max}$ for ionization chambers in electron beams." *Med Phys* 26:208–213.

Rogers, D. W. O. (2004). "Accuracy of the Burns equation for stopping-power ratio as a function of depth and R_{50}." *Med Phys* 31:2961–2963.

Rogers, D. W. O. (1999). "Correcting for electron contamination at dose maximum in photon beams." *Med Phys* 26:533–537.

Rogers, D. W. O. (1998). "A new approach to electron beam reference dosimetry." *Med Phys* 25:310–320.

Rogers, D. W. O. "Fundamentals of Dosimetry Based on Absorbed-Dose Standards" in *Teletherapy: Present and Future*. J. R. Palta and T. R. Mackie (eds.). Madison, WI: Advanced Medical Physics, pp. 319–356, 1996.

Rogers, D. W. O. (1992a). "Calibration of parallel–plate ion chambers: Resolution of several problems by using Monte Carlo calculations." *Med Phys* 19:889–899.

Rogers, D. W. O. (1992b). "The advantages of absorbed-dose calibration factors." *Med Phys* 19:1227–1239.

Rogers, D. W. O. "Fundamentals of High Energy X-ray and Electron Dosimetry Protocols" in *Advances in Radiation Oncology Physics,* J. Purdy (ed.). Medical Physics Monograph 19. New York: American Institute of Physics, pp. 181–223, 1992c.

Rogers, D. W. O. (1991). Compilation of Quantities Associated with Dosimetry Protocols. NRC Report PIRS–291. Ottawa: NRC.

Rogers, D. W. O., and A. F. Bielajew. (1986). "Differences in electron depth dose curves calculated with EGS and ETRAN and improved energy range relationships." *Med Phys* 13:687–694.

Rogers, D. W. O. and A. Booth. (2009). PROT: A General Purpose Utility for Calculating Quantities Related to Dosimetry Protocols. Technical Report CLRP 09-01, PIRS–529 (rev. in preparation). Ottawa: Carleton University and National Research Council.

Rogers, D. W. O., and C. K. Ross. (1992). "Comparison of IAEA 1987 and AAPM 1983 protocols for dosimetry calibration of radiotherapy beams." *Med Phys* 19:213–214.

Rogers, D. W. O., and C. K. Ross. (1988). "The role of humidity and other correction factors in the AAPM TG–21 dosimetry protocol." *Med Phys* 15:40–48.

Rogers, D. W. O., and C. L. Yang. (1999). "Corrected relationship between $\%dd(10)_x$ and stopping-power ratios." *Med Phys* 26:538–540.

Rogers, D. W. O., B. A. Faddegon, G. X. Ding, C.-M. Ma, J. Wei, and T. R. Mackie. (1995). "BEAM: A Monte Carlo code to simulate radiotherapy treatment units." *Med Phys* 22: 503–524.

Rogers, D. W. O., C. K. Ross. K. R. Shortt, N. V. Klassen, and A. F. Bielajew. (1994). "Towards a Dosimetry System Based on Absorbed-Dose Standards" in Proceedings of a Symposium on Measurement Assurance in Dosimetry, pp. 565–580. IAEA–SM–330/9. Vienna, Austria: IAEA.

Ross, C. K., K. R. Shortt, D. W. O. Rogers, and F. Delaunay. (1994). "A Test of TPR_{10}^{20} as a Beam Quality Specifier for High-Energy Photon Beams" in Proceedings of a Symposium on Measurement Assurance in Dosimetry, pp. 309–321. IAEA–SM–330/10. Vienna, Austria: IAEA.

Schulz, R. J., P. R. Almond, G. Kutcher, R. Loevinger, R. Nath, D. W. O. Rogers, N. Suntharalingham, K. A. Wright, and F. Khan. (1986). "Clarification of the AAPM Task Group 21 protocol." *Med Phys* 13:755–759.

Seltzer, S. (2008). NIST, private communication.

Seuntjens, J. P., C. K. Ross, K. R. Shortt, and D. W. O. Rogers. (2000). "Absorbed-dose beam quality conversion factors for cylindrical chambers in high-energy photon beams." *Med Phys* 27:2763–2779.

Sheikh-Bagheri, D., D. W. O. Rogers, C. K. Ross, and J. P. Seuntjens. (2000). "Comparison of measured and Monte Carlo calculated dose distributions from the NRC linac." *Med Phys* 27:2256–2266.

Shiragai, A. (1979). "Effective mass stopping power ratio in photon dosimetry." *Phys Med Biol* 24:452–454.

Shiragai, A. (1978). "A proposal concerning the absorbed dose conversion factor." *Phys Med Biol* 23:245–252.

Spencer, L. V., and F. H. Attix. (1955). "A theory of cavity ionization." *Radiat Res* 3: 239–254.

Svensson, H., and A. Brahme. "Recent Advances in Electron and Photon Dosimetry" in *Radiation Dosimetry.* C. G. Orton (ed.). New York: Plenum Press, pp. 87–170, 1986.

Thwaites, D. I., D. T. Burns, S. C. Klevenhagen, A. E. Nahum, and W. G. Pitchford. (1996). "The IPEMB code of practice for electron dosimetry for radiotherapy beams of initial energy from 2 to 50 MeV based on air kerma calibration." *Phys Med Biol* 41:2557–2603.

Titt, U., O. N. Vassiliev, F. Ponisch, L. Dong, H. Liu, and R. Mohan. (2006). "A flattening filter free photon treatment concept evaluation with Monte Carlo." *Med Phys* 33(6): 1595–1602.

Van der Plaetsen, A., J. Seuntjens, H. Thierens, and S. Vynckier. (1994). "Verification of absorbed doses determined with thimble and parallel-plate ionization chambers in clinical electron beams using ferrous sulphate dosimetry." *Med Phys* 21:37–44.

Verhaegen, F., R. Zakikhani, A. DuSautoy, H. Palmans, G. Bostock, D. Shipley, and J. Seuntjens. (2006). "Perturbation correction factors for the NACP-02 plane-parallel ionization chamber in water in high-energy electron beams." *Phys Med Biol* 51:1221–1235.

Wang, L. L. W., and D. W. O. Rogers. (2009a). "Study of the effective point of measurement for ion chambers in electron beams by Monte Carlo simulation." *Med Phys* 36:2034–2042.

Wang, L. L. W., and D. W. O. Rogers. (2009b). "The replacement correction factors for cylindrical chambers in electron beams." *Med Phys* 36 (to be submitted, Jan. 2009).

Wang, L. L. W., and D. W. O. Rogers. (2009c). "The replacement correction factors for cylindrical chambers in high-energy photon beams." *Phys Med Biol* 54:1609–1620.

Wang, L. L. W., and D. W. O. Rogers. (2008a). "Calculation of the replacement correction factors for ion chambers in megavoltage beams by Monte Carlo simulation." *Med Phys* 35:1747–1755.

Wang, L. L. W., and D. W. O. Rogers. (2008b). "The replacement correction factor for the BIPM flat cavity ion chamber and the value of *W*/*e*." *Med Phys* 35:4410–4416.

Weinhous, M. S., and J. A. Meli. (1984). "Determining P_{ion}, the correction factor for recombination loses in an ionization chamber." *Med Phys* 11:846–849.

Wittkämper, F. W., H. Thierens, A. Van der Plaetsen, C. de Wagter, and B. J. Mijnheer. (1991). "Perturbation correction factors for some ionization chambers commonly applied in electron beams." *Phys Med Biol* 36:1639–1652.

Wulff, J., J. T. Heverhagen, and K. Zink. (2008). "Monte-Carlo-based perturbation and beam quality correction factors for thimble ionization chambers in high-energy photon beams." *Phys Med Biol* 53:2823–2836.

Wulff, J., K. Zink, and I. Kawrakow. (2008). "Efficiency improvements for ion chamber calculations in high energy photon beams." *Med Phys* 35:1328–1336.

Xiong, G., and D. W. O. Rogers. (2008). "Relationship between $\%dd(10)_x$ and stopping-power ratios for flattening filter free accelerators: A Monte Carlo study." *Med Phys* 35: 2104–2109.

Zink, K. and J. Wulff. (2008). "Monte Carlo calculations of beam quality correction factors k_Q for electron dosimetry with a parallel-plate Roos chamber." *Phys Med Biol* 53: 1595–1607.

Problems

1. Derive equation (9.9) for $N_{D,w}^{Q_{ecal}}$ and equation (9.10) for $N_{D,w}^{Q}$ in an electron beam of quality R_{50} starting from the earlier equations.

2. Derive equation (9.14) for the dose to the medium in terms of D_{air}.

3. Starting from the definition of P_{gr} and assuming that $D(z) = D_o e^{-\mu' z}$ for all depths z past the depth of dose maximum, derive equation (9.39) for P_{gr}^{offset} in terms of the offset Δz.

4. Starting from equation (9.41), derive equation (9.42) for P_{ion} for general recombination in a continuous beam.

5. Starting from equation (9.43), derive equation (9.46) for P_{ion} in a pulsed beam.